WEATHERING OF DEEP-SEA HYDROTHERMAL SULFIDE DEPOSITS

STABILITY OF HEAVY METALS AND IMPLICATIONS FOR FUTURE MINING ACTIVITIES

MASTER OF SCIENCE THESIS

LINN MERETHE BREKKE OLSEN

Department of Earth Science

University of Bergen, Norway

December 2016

Abstract

During future mining operations on seafloor massive sulfide deposits, sulfidic material will be reworked and relocated at the seafloor, exposing the material to oxic conditions. In an oxic environment sulfidic material will weather through oxidation, a microbial catalyzed process that is well known from on-land mining activities to result in acidic conditions and increased solubility of heavy metals in the aquatic phase. However, few studies have addressed the role of microbial processes in weathering of deep-sea hydrothermal deposits, and how these processes affect the mobility of heavy metals in the marine environment. This study has investigated the mobility of heavy metals in the Loki's Castle hydrothermal mound and the background sediment by geochemical analysis of the solid material and extracted pore-water from two push cores, combined with microbial DNA analysis of the two materials. The mound material was anoxic, with pore-water concentrations of Zn, Cu and Pb in range of 7-29, 2-10, and 0-0.4 ppb, whilst the solid phase concentrations ranged from 2120-8030, 3920-6650 and 347-650 ppm, respectively. Solid phase concentrations were lower in the oxic background sediment, with Zn in range of 108-274 ppm, and Cu and Pb ranged from 81-686 and 23-178 ppm, whilst pore-water concentrations of Zn, Cu and Pb ranged from 4.6-37, 2.7-8 and 0-1.3 ppb. The heavy metals in the mound material are derived from mineral precipitated by seawater and hydrothermal fluid mixing, leading to precipitation of various metal bearing minerals, whilst the background sediment consists mainly of pelagic and glaci-marine sediment with a layer composed of hydrothermal fall out material. The microbial community in the mound material consisted of a high relative abundance of SO_4^{2-} reducers, Fe reducers and anaerobic sulfur oxidizers, whilst the background sediment had a high relative abundance of aerobic NH_3 and NO_2 oxidizers. The heavy metal concentrations in pore-water from the anoxic mound material were expected to be higher compared to the concentrations in the oxic background sediment, since the mound material had a higher heavy metal content in the solid phase, and the similar pore-water concentrations were therefore unexpected. The reduction of metal oxyhydroxides and the oxidation of sulfides release heavy metals to the pore-water, and the difference in relative mobility of the heavy metals in the two sediment cores is suggested to be related to the relative abundance of SO_4^{2-} reducing microorganisms in the mound material, which by producing H_2S immobilize the heavy metals due to secondary precipitation of metal sulfides. The lack of SO_4^{2-} reducers in the background sediment show that the heavy metal concentrations

must be controlled by other processes, possibly by adsorption to other minerals (clays and oxides) or concomitant precipitation of metal oxides. The exposure of sulfidic material to oxic conditions during mining activities will oxidize the sulfides and release the heavy metals to the aquatic phase, and since the process of immobilizing heavy metal seems to be less efficient in an oxic compared to an anoxic environment, an increase of heavy metals in the aquatic phase is expected to occur.

Acknowledgments

This study has been financed by the Centre for Geobiology (CGB) at the University of Bergen and the Managing Impacts of Deep-sea Resource Exploitation (MIDAS) project.

To the people connected to Centre for Geobiology, I owe you all a big thank you. Rolf B. Pedersen, for being responsible for gathering the material building the foundation for this study; the two sediment push-cores sampled during the Centre for Geobiology research cruise 2015. Ingunn Thorseth and Ingeborg Økland, thank you for a good guidance over the last years. Ingunn, you know what to do to get the best final product possible, which have pushed me even longer. A very special thanks to Ingeborg, who has not only been a good supervisor, but also been a good friend. You know exactly how to motivate me, and how to guide me the best possible way. Anita-Elin Fedøy, for all the help in the lab during extraction and PCR amplification and Haakon Dahle for classification of the sequences obtained and for pointing me in the right direction when interpreting and presenting my results. Cédric Hamelin for showing me how I can combine different computer programs to set my ideas to life regarding graphs and figures. Pål Tore Mørkved, Runar Stokke, Eoghan Reeves, Desiree Roerdink, Irene Roalkvam, Filipa Marquez and others not mentioned, all of you have answered my numerous questions I have been thinking about the last two years.

I would also like to thank Hildegunn Almelid and Siv Hjort Dundaas for pore-water analysis, Ole Tumyr and Trygve Knag for XRD analysis and guidance in the interpretation work. Irina Dimitru and Martina Hamre for guidance while preparing my samples for geochemical analysis, and my good friends Jamie Taylor, for reading and correcting my text.

To my fellow students, friends and family not mentioned previously; thank you for the support I have received. The financial support, and encouraging words from my family, and also from my fellow students and close friends have helped me in times were my motivation was lacking.

Table of Contents

1 Introduction

Mining of high grade ores to obtain valuable quantities of essential and precious metals will always be an important industry in our society. The increasing demand for these metals has lead the industry to explore the possibility of exploitation in the deep-sea, with seafloor massive sulfide (SMS) deposits as a possible future resource (Hoagland et al., 2010; Petersen et al., 2016; Rona, 2003). SMS deposits are iron, copper, zinc, lead and sulfur-rich mineral deposits that precipitate from hydrothermal fluids as they mix with the cooler ambient seawater at or beneath the seafloor at hydrothermal vent sites (Hoagland et al., 2010). These type of deposits can contain high concentrations of commercially valuable elements. An example of such a deposit is Solwara 1 in the Eastern Manus Basin which contains large amounts copper and gold, and where commercial exploitation is under planning (Nautilus Mineral Inc, 2016).

Regulations and baselines regarding the environmental impact of deep-sea mining has not yet been developed, and an evaluation of the environmental impacts in the case of exploitation is needed (Rona, 2003; Van Dover, 2011). In the planned exploitation in the Solwara 1 project, 130.000 tons of unconsolidated sediment and 115.000 tons of competent waste material is planned to be evenly dispersed out on the seafloor, and during ore extraction, 10% of the exploited ore material lost on the seafloor during the operation will not be retrieved due to equipment flaws. No geochemical modeling on how weathering proceeds have been performed on the material that stays at or close to the seafloor during and after the operation, since the material is assumed to be stable at these environmental conditions (Nautilus Mineral Inc, 2016). An assessment of the long term impacts, including geochemical changes, is so far inadequate in these parts of the operation. The weathering processes in hydrothermal sulfide deposits can be considered as natural analogs to how the processes that is expected to proceed during seafloor mining. However, as detection of SMS deposits is commonly based on methods only applicable to active vent sites (e.g. plume detection), the scientific information on non-active hydrothermal deposits on the seabed is lacking, making the characterization of potential environmental effects of mineral exploitation difficult (Hoagland et al., 2010).

In on-land mining, one of several well-known environmental impacts is the generation of acid mine drainage (AMD) and the mobilization of metal(loids) during weathering of sulfides, a process which can contaminate ground, surface and nearby marine waters (Carr et al., 2003; Lindsay et al., 2015; Moncur et al., 2005, 2009; Nordstrom, 2011). In an attempt to reduce the oxidation of sulfide minerals, seafloor tailing deposits (STD) have been used as an alternative to land based mine tailing deposition. It is assumed that the stability of tailings in the marine environment will be higher, since low O_2 concentrations in the bottom waters will minimize oxidation, and the higher pH and the buffer capacity of seawater will immobilize the potentially released heavy metals (Dold, 2014). Some of the known environmental disadvantages of STDs include the bioaccumulation of metals through the food chain, liberation of toxic elements from tailings to the seawater, and physical and geochemical alteration of the bottom habitat (Dold, 2014). Weathering of sulfides includes a range of different reactions, and microbial activity may play an important role in the mobilization or immobilization of heavy metals. How these processes occur in hydrothermal deposits in the marine environment has received limited attention, however, more knowledge about how the biogeochemical processes proceeds in such a deposit can be useful when estimating the environmental impacts of deep-sea mining.

1.1 Sulfide weathering and associated chemolithotrophic microorganisms

Weathering of sulfides includes two processes, dissolution and oxidation. Under reducing conditions sulfides are regarded as thermodynamically stable minerals with low solubility. On the other hand, when exposed to for example Fe^{3+} and O_2 they will oxidize, as shown in Eq.1. with pyrite (FeS_2) as an example (Moses et al., 1987; Singer and Stumm, 1970).

$$FeS_{2(s)} + H_2O + 3.5O_2 \rightarrow Fe^{2+} + 2SO_4^{2-} + 2H^+ \quad \text{(Eq.1)}$$

$$Fe^{2+} + 0.25\ O_2 + H^+ \rightarrow Fe^{3+} + 0.5\ H_2O \quad \text{(Eq.2)}$$

$$FeS_{2(s)} + 14Fe^{3+} + 8H_2O \rightarrow 15Fe^{2+} + 2SO_4^{2-} + 16H^+ \quad \text{(Eq.3)}$$

The oxidation of pyrite will release Fe^{2+}, which can be oxidized to Fe^{3+} by available O_2 (Eq.2). Ferric iron is itself an active oxidizer (Eq.3), and in a low pH environment Fe^{3+} will oxidize pyrite with a higher rate than O_2 (Singer and Stumm, 1970). The oxidation of dissolved Fe^{2+} by O_2 (Eq.2) is the rate-limiting step in the general process, and the rate decreases with decreasing pH (Singer and Stumm, 1970). However, the process is accelerated by microbial activity, and microbial

oxidation of Fe^{2+} produce Fe^{3+} that will work as an oxidizer as rapidly as the microorganism can generate it (Nordstrom and Southam, 1997; Singer and Stumm, 1970). In a neutral, oxygenated environment the rapid autooxidation of Fe^{2+} is thought to inhibit the microorganisms ability to oxidize Fe^{2+}. An in-situ alteration study of sulfide materials in oxygenated marine environments by Edwards et al., (2003, 2004) suggests that the spatial heterogeneity of cells and oxides on chimney sulfides are related to the development of microaerophilic environments in pits and pores of the materials, supporting the growth of neutrophilic Fe-oxidizing microorganisms by suppressing the rapid abiotic autooxidation reaction at these conditions.

Ferric iron has a low solubility at circumneutral pH, but a study by Moses and Herman (1991) suggests a mechanism where Fe^{3+} works as an active oxidizer also at these conditions. The model suggests that electrons are transferred from the pyrite surface to Fe^{3+} by producing Fe^{2+} on the mineral surface, which is then oxidized by dissolved O_2 in the aqueous phase.

Oxidation by O_2, and subsequent generation of Fe^{3+} is also the pathway for pyrrhotite ($Fe_{(1-x)}S$) (Eq.4, Eq.5) (Janzen et al., 2000) and sphalerite ($Zn_{(1-x)}Fe_x)S$) (Eq.6) (Moncur et al., 2005) (Eq.7) (Rimstidt et al., 1993) oxidation.

$$Fe_{(1-x)}S_{(s)} + (2 - 0.5x)O_2 + xH_2O \rightarrow (1 - x)Fe^{2+} + SO_4^{2-} + 2xH^+ \quad \text{(Eq.4)}$$

$$Fe_{(1-x)}S_{(s)} + (8 - 2x)Fe^{3+} + 4H_2O \rightarrow (9 - 3x)Fe^{2+} + SO4_4^{2-} + 8H^+ \quad \text{(Eq.5)}$$

$$(Zn_{(1-x)}Fe_x)S_{(s)} + 2O_2 \rightarrow (1 - x)Zn^{2+} + xFe^{2+} + SO_4^{2-} \quad \text{(Eq.6)}$$

$$(Zn_{(1-x)}Fe_x)S_{(s)} + 8Fe^{3+} + 4H_2O \rightarrow (1 - x)Zn^{2+} + (8 + x)Fe^{2+} + SO_4^{2-} + 8H^+ \quad \text{(Eq.7)}$$

The weathering process of these three sulfides (Eq.1, Eq. 3-Eq.7) shows how oxidation of sulfides can generate acid and/or SO_4^{2-}. The oxidation of pyrrhotite might be incomplete, with only parts of the sulfide being completely oxidized to SO_4^{2-} combined with production of elemental sulfur or an increasingly sulfur-rich pyrrhotite (Janzen et al., 2000). Pyrrhotite (Janzen et al., 2000) and sphalerite (Crundwell and Verbaan, 1987) are also regarded as acid soluble, and can dissolve without oxidation. Sulfide oxidation is not only due to the process of iron oxidation with O_2 as an electron acceptor. Sulfide and sulfur oxidizing microorganisms can oxidize sulfide as part of their chemolithoautotrophic metabolism, where they oxidize inorganic substances to gain energy with other terminal electron acceptors than O_2 (e.g. Konhauser, 2007). One example is members

belonging to the *Sulfurimonas* genus, which can oxidize sulfide with different types of electron acceptors, such as NO_3^-, and is thereby not dependent on the presence of O_2 (Inagaki, 2003; Takai, 2006).

During weathering the metal(loids) and related trace elements can be mobilized in the surrounding aquatic phase (Carr et al., 2003; Lindsay et al., 2009; Moncur et al., 2005; Smuda et al., 2007). For instance, pyrite can contain various elements (e.g. As, Cu, Pb, Zn) in major or trace concentrations (Abraitis et al., 2004), sphalerite can be the main contributor of Cd (Moncur et al., 2005; Smuda et al., 2007) and possibly As and Se (Labrenz et al., 2000) and pyrrhotite can contain e.g. Co, Mn, Ni and Cu (Janzen et al., 2000). The concentration of the related trace elements in the surrounding waters depends on the concentration in the primary sulfide, the mass of it, and the extent of secondary reactions following the dissolution. Subsequent precipitation and dissolution, reduction and oxidation, and sorption and desorption reactions in the system controls the pore-water pH and the mobility of the weathering products (Lindsay et al., 2009, 2015; Moncur et al., 2005; Sidenko and Sherriff, 2005; Smuda et al., 2007). A study by Smuda et al., (2007) shows that heavy metals can be enriched in secondary precipitates within altered rocks and then later be mobilized depending on the solubility of the secondary minerals. As a general example, the precipitation of Fe^{3+} hydroxide in relation to oxidation of pyrite is presented in Eq.8 and the overall reaction in Eq.9 (Nordstrom, 1982)

$$Fe^{3+} + 3H_2O \rightarrow Fe(OH)_{3(s)} + 3H^+ \quad \text{(Eq.8)}$$

$$FeS_2 + 15/4O_2 + 7/2H_2O \rightarrow Fe(OH)_{3(s)} + 2SO_4^{2-} + 4H^+ \quad \text{(Eq.9)}$$

The precipitation of Fe^{3+} hydroxides can work as a solid phase control on mobilized elements due to precipitation or adsorption, e.g. of zinc (Moncur et al., 2005) or arsenic (Smuda et al., 2007). The production of Fe^{3+} oxyhydroxides can also be induced by microbial oxidation of Fe^{2+}. This process is thought to explain the presence of large mats of Fe^{3+} oxyhydroxides in hydrothermal environments where the hydrothermal fluids is enriched in Fe^{2+} (e.g. Emerson and Moyer, 2002)

1.2 Biogeochemical processes in marine sediment

The effect of microbial activity on mineral precipitation and pore-water geochemistry is especially notable in the marine environment during degradation of organic matter. Newly deposited sediment consisting of inorganic detritus, organic matter and pore-water is affected by the conversion of

organic matter to CO_2 and CH_4 as part of the diagenetic process, where microorganisms reduce inorganic substances while oxidizing organic matter to obtain energy for growth. This process proceeds in a continuous series of redox reactions, where the electron acceptor with the highest free energy yield is used as the terminal electron acceptor (Fig.1). The successive microbial reduction of dissolved O_2 and NO_3^-, solid Mn and Fe oxyhydroxides, and SO_4^{2-}, and CO_2 in the sediment leads to the generation of different byproducts (e.g. HCO_3-, Mn^{2+}, Fe^{2+}, NH^{4+}, NO_2, HS^-, HPO_4^{2-} and CH_4) in the pore-water. The dissolved species can successively lead to the precipitation of secondary minerals (Konhauser, 2007). These processes are consequently very important for the mobility of the elements in the sediment. One example is the microbial reduction of metal oxyhydroxides that release Fe and Mn to the pore-water (Fig.1). The mobilized elements can subsequently be immobilized through microbial induced sulfide precipitation, a process dependent on SO_4^{2-} reduction. Sulfate reducing microorganisms in anoxic environments can use SO_4^{2-} as a terminal electron acceptor for the degradation of organic compounds, resulting in the production of hydrogen sulfide (H_2S) (Muyzer and Stams, 2008; Offre et al., 2013), which, in the presence of dissolved metal species, can lead to precipitation of corresponding metal sulfides, e.g. CuS, FeS, ZnS (Dvorak et al., 1991; Ehrlich, 1999; Labrenz et al., 2000). The process of SO_4^{2-} reduction is an important process when it comes to immobilizing metals, and is used in treatments of mine drainage with an increased metal concentration (Dvorak et al., 1991; Jong and Parry, 2003; Kaksonen and Puhakka, 2007).

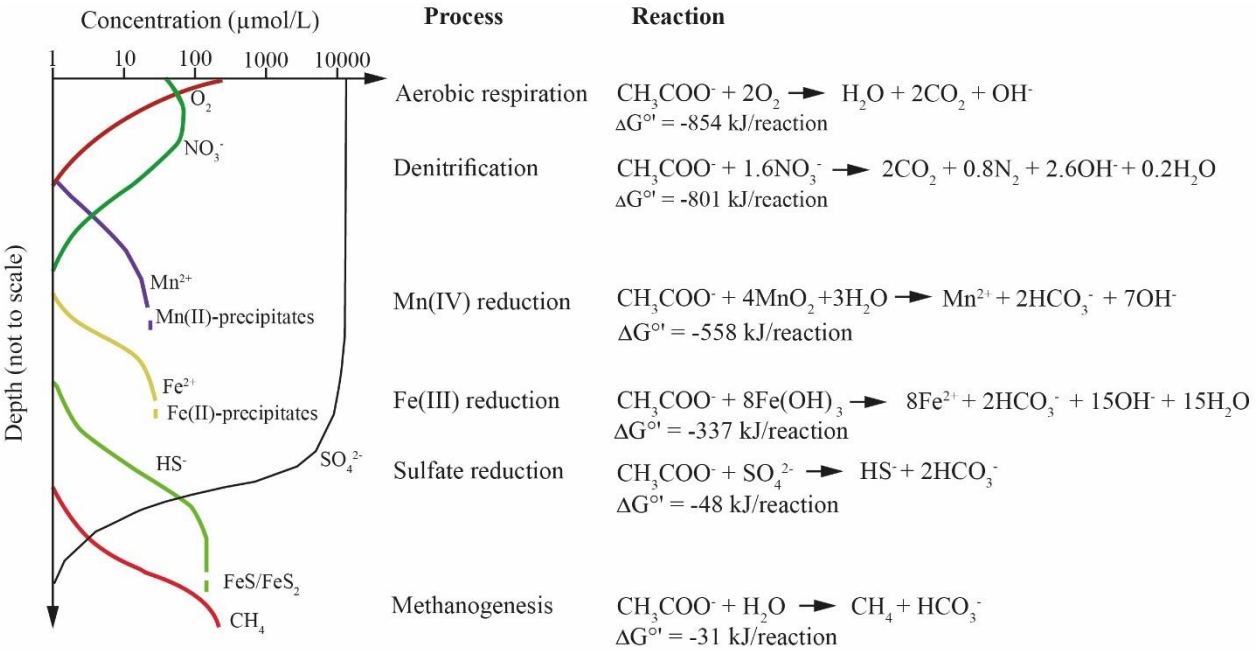

Figure 1: Idealized pore-water and solid phase profiles based on the successive utilization of terminal electron acceptors during the decomposition of marine sedimentary organic matter. Modified from the adapted Froelich et al., (1979) as presented in Konhauser (2007).

1.3 Aim of study

The aim of this study was to determine important weathering reactions in the arctic Loki's Castle hydrothermal sulfide deposits, with a special focus on the major biogeochemical processes important for the mobility of heavy metals, and the potential impacts of these processes in future deep-sea mining operations. The study combines geochemical analyses of pore-water and sediment with microbial community analysis on sediment cores. One sediment core was sampled from within the sulfide mound surrounding the hydrothermal vent field Loki's Castle, and one sediment core was sampled from the outside of this mound. The study is a part of the Managing Impacts of Deep-sea Resource Exploitation (MIDAS) project (EU-FP7).

2 Materials and method

2.1 Study site

Loki's Castle is an active hydrothermal vent field located at the slow-spreading Arctic Mid-Ocean Ridge, where the Mohns Ridge passes into the Knipovich Ridge (Fig.2a, b)(Pedersen et al., 2010a). The field is characterized as a sedimentary influenced basalt-hosted system, where the sediment is inferred to be glaci-marine sediment derived from the Bear Island Fan (Fig.2b) (Pedersen et al., 2010a; Baumberger et al, 2016a, 2016b) The field consists of four active black smoker chimneys with fluids reaching a temperature of 310-320°C, where three chimneys are located closely together and one 150 m eastward from these. The main sulfide assemblage in the chimneys is sphalerite, pyrite and pyrrhotite and minor amounts of chalcopyrite. Around the venting areas there is a build-up of two 20-30 m high sulfide mounds. The two mounds are 150-200 m across at the base where they coalesce into a large composite mound, mainly composed of chimney debris and hydrothermal plume material (Pedersen et al., 2010a, 2010b).

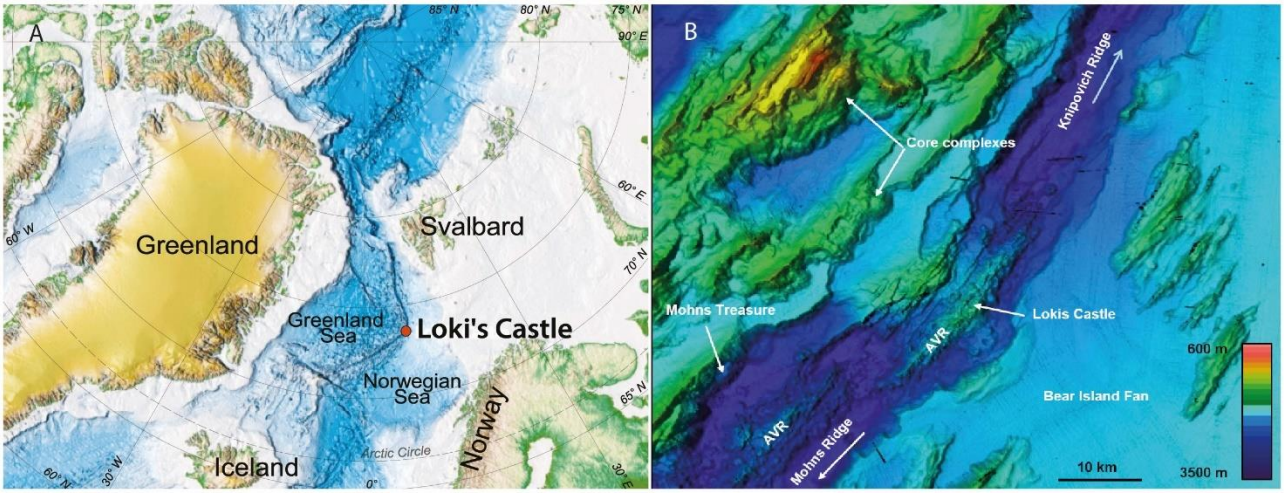

Figure 2: A. Map showing the location of the active hydrothermal vent field Loki's Castle, at the Arctic Mid Ocean Ridge (AMOR). B. Bathymetric map showing the location of Loki's Castle on a volcanic ridge (AVR) in the rift valley, and its proximity to the Bear Island Fan. Modified from Pedersen et al., (2010a).

2.2 Sampling

Two push-cores were collected by the ROV "Ægir 6000" at the Loki's Castle vent field during a research expedition with R/V G.O Sars in June-July 2015, where core 1 (GS15-ÆGIR08-PC1) was from the eastern flank of the sulfidic mound (73°34.019 N, 8°09.535 E; 2350 m depth) and core 2 (GS15-ÆGIR08-PC2) was from outside the mound (73°34.021N, 8°09.872 E; 2362 m depth) approximately 520 m east of core 1. After retrieval, the sediment cores were split in half, and samples for DNA and pore-water analysis were collected. The cores were wrapped in plastic, and core 1 was flushed with nitrogen gas and sealed in a plastic sleeve to avoid further oxidation. Both cores were stored at 4°C.

2.3 Methods

X-ray diffraction (XRD) analysis was performed by an Eco D8 Advance (BRUKER) on sediment samples from 1, 2, 12, 20 and 25 cm depth of core 1. The samples were dried at 105°C before being crushed by hand using an agate mortar and evenly dispersed on a glass plate. A corundum standard was analyzed in each run using 40kV and 40mA with an angle rom 5-70°. The software DIFFRAC.EVA V4.1.1 and the Crystallography Open Database (COD) was used to analyze the obtained spectra by comparing them spectra in the database of minerals commonly found in hydrothermal deposits, known alteration products and various sulfides known to derive from biological activity. The different clay mineral groups were identified by re-analyzing the sediment samples after glycolation for 14 hours at 60°C, and after successively heating for 2 hours at 300-350°C and 500-600°C, at an angle of 4.5-31°, and compared to the observed changes of the spectra between the different steps with the characteristic behavior of different clay mineral groups according to Table 1 (Thorez, 1975, and refs. therein)

Table 1: Characteristic peaks for the clay mineral groups in untreated samples, and after glycolation and heating.

	Untreated	Glycolation:	300-350°C	Heating 500-600°C
Kaolinite	7Å, 12.6°	7Å, 12.6°	7Å, 12.6°	-
Smectite	12-15Å, 7.3-5.9°	17Å, 5.2°	10Å, 8.8°	10Å, 8.8°
Illite	10Å, 8.8°	10Å, 8.8°	10Å, 8.8°	10Å, 8.8°
Chlorite	14Å, 6.3°	14Å, 6.3°	14Å, 6.3°	14Å, 6.3°

Sediment for scanning electron microscopy (SEM) was collected at 1, 2, 12, 20 and 25 cm depth of core 1 immediately after retrieval, and stored in a 2.5% glutaraldehyde seawater solution at 4°C until analysed. The samples were dehydrated in an ethanol series (1x50%, 1x75%, 3x96%, 10 min each) on 0.2 µm polycarbonate filters. The filters were then air-dried, mounted on aluminum stubs using carbon tape, and coated with iridium using a Gatan Precision Etching Coating System (Model 682), or by carbon using an Agar Turbo Carbon Coater. The samples were investigated by Zeiss Supra™ – 55V Field Emission SEM (Gemini) equipped with a Thermo Noran System 7 energy dispersive X-ray spectrometer (EDS) system.

The sediment geochemistry of core 2 was first analyzed with an Itrax X-Ray fluorescence (XRF) Core Scanner (Cox Analytical Systems) with 200 µM resolution. The results from the XRF scan were then used to select discrete sediment samples for quantitative geochemical analysis from 0-1.5, 8-9, 16-17, 21-22 and 40-41 cm depth. In addition, discrete samples from 0-1.5, 10-11 and 21-22 cm depth in core 1 were also collected. The sediment samples were dried at 105°C and crushed by an agate ball mill (Retsch MM200) for 6 minutes at a frequency of 30 hertz. The samples were analyzed by Actlabs (Toronto, Canada) for concentrations of major and trace elements and to determine the total sulfidic sulfur content. Sample preparation for major oxides and selected trace elements (Ba, Be, Sc, Sr, V, Y, Zr) was done by lithium metaborate/tetraborate fusion followed by a weak nitric acid solution digestion, before analyzed by inductively coupled plasma-optical emission spectroscopy (ICP-OES) on Thermo Jarrell – Ash ENVIRO II or Varian Vista 735 ("Lithogeochemistry-Geochemistry | Actlabs"). Additional trace element analysis on base metals (Ag, Cd, Cu, Ni Pb, S, Zn) was done using a four acid-digestion treatment before analyzed by Varian Vista 735, using in-lab standardstraceable to certified reference material (USGS or CANMET) ("Total Digestion-ICP-Geochemistry / Assay | Actlabs,"). Instrumental Neutron Activation Analysis (INAA) was used to analyze As, Au, Br, Ce, Co, Cr, Cs, Eu, Hf, Ir, La, Lu, Mo, Nd, Rb, Sb, Se, Sm, Ta, Tb, Th, U, W and Yb, (Hoffman, 1991) with an in-lab standard run every 11 sample. Sulfidic sulfur concentrations were analyzed by the calculated difference between measurements at 550°C and 1450°C by using a combustion/IR, pyrolysis loss sulfur ("Sulphide-Geochemistry / Assay | Actlabs,"). Totals outside 98.5-101% indicate the presence of sulfate, Li or other elements not analyzed for ("Lithium Metaborate/Tetraborate Fusion-ICP-Geochemistry / Assay | Actlabs,"). Sediment from the same depths were dried at 105°C and crushed by hand by an agate mortar before being analyzed for total organic carbon (TOC) content by an element analyzer

(Multi EA 4000, Analytik Jena AG). The method was calibrated with a calcium carbonate standard, and recalibrated after every 10th analysis.

Pore-water was extracted from the two cores short time after retrieval using Rhizon samplers with a 0.15 µM pore size (Rhizosphere Research Products). The pore-water was extracted from 1-3, 7-8, 12-14 and 18-20 cm depth of core 1, and from 2-4, 9-11, 18-21, 29-31, 39-41 and 45-47 cm depth of core 2. In addition, bottom seawater from the water above the core surface in the core liners. pH and alkalinity were analyzed with an 826 pH Mobile (Metrohm) meter and a 888 Titrando (Metrohm) titrater onboard the research vessel. H_2S, NH_4, NO_3, NO_2 and PO_4 were analyzed colourmetrically by a semi-automated Quaatro Analyzer (Seal) shipboard immediately after sampling. Samples for ICP-OES and ICP-mass spectrometry (MS) were acidified to 3vol % HNO_3 and stored in acid – washed high density poly ethylene (HDPE) bottles at 4°C until analyzed. Major elements were analyzed by ICP-OES (iCAP7000 series, Thermo Scientific) whilst trace elements where analyzed by ICP-MS Element XR (Thermo Scientific). Samples for ionechromotographic (IC) analysis were stored in regular HDPE bottles at 4°C until analyzed by an Methrom IC.

Sediment for microbial community analysis was sampled at various depths (Appendix B) in the two sediment cores using sterile spatulas immediately after retrieval. They were stored in sterile syringes and cryo-tubes at -80°C until further analysis. DNA was extracted using the Fast DNA Spin Kit (MP Biomedicals, Lot.nr 68505) for soil in conjunction with FastPrep 24 instrument (MP Biomedicals, Santa Ana, CA, USA) (Appendix C). Because of unquantifiable results in the first attempt to isolate DNA from the core sampled in the sulfide mound (core 1), samples from core 1 were treated with poly deoxyinosinic-deoxytidylic acid or poly adenosine, before isolating the DNA. 0.25-0.5g of sediment from 0.1 and 1 cm depth in core 1 were placed in a sterile 2.0 ml micro-centrifuge tube containing 250 µl of solution (200 mM Tris, 50 mM EDTA, 200 mM NaCl) containing either 2 µl poly deoxyinosinic-deoxytidylic acid or 10 µl poly adenosine, and incubated over night at 4°C. The procedure was presented by Brazelton et al., (2010), where they used poly deoxyinosinic-deoxytidylic acid before DNA extraction. After running a PCR1 test run after DNA extraction, it was decided to only continue with the poly adenosine treatment on the samples from core 1, and out of the results presented only one sample have been pre-treated with poly deoxyinosinic-deoxyidylic acid. The extraction of DNA from the background core (core 2) was

performed without deoxyinosinic-deoxytidylic acid or poly adenosine treatment. After storage at -20°C, the isolated DNA templates were amplified by a two-step PCR approach using universal 16S rRNA primers targeting the V4 region (519F-and 806R), together with HotStarTaq® PCR kit (Qiagen) (Appendix C). The PCR product was sequenced by Ion Torrent (Life Technologies), and the sequences obtained were classified using either GreenGenes or Silva database. Analyses with <1500 reads in total were excluded as reliable results. A blank from Fast DNA Spin Kit went through the same procedure to detect possible contamination.

3 Results

Core 1 collected from the mound was approximately 30 cm long (Fig.A-1). The core had a rusty layer in the top few millimeters. Within the deeper parts of the core there was alternating layers of rusty and dark brown and dark grey material. The grain size was mainly clay to sand, but layers of unconsolidated coarser material, up to 2 cm, were found within patches of the core. The core smelled of H_2S when retrieved.

Core 2 from the background sediment was approximately 50 cm long (Fig.A-2), and contained alternating light grey to light brown layers of clay and silt.

3.1 Mineralogy of the sulfide mound (core 1)

The results from the XRD analysis of core 1 indicated different mineralogical phases with various degree of crystallinity, especially notable for the uppermost sediment sample. Inspection by SEM-EDS analysis indicated a higher concentration of sulfides in the deepest part of the core (25 cm depth). The sulfides detected include various Zn, Cu and Fe sulfides with minor content of other elements in their composition (e.g. Ag, Ga, Pb, Ni, Cd), and with different morphologies (Fig.3 a-e).

Table 2: Selected sulfides tested against the XRD spectra at different depths in the core. Moderate match indicates a likely presence. Sulfides with a strong match are presented as part of the sulfide assemblage.

Depth	*0-1.5 cm*	*2 cm*	*12 cm*	*20 cm*	*25 cm*
Pyrite (FeS_2)	Moderate	-	Moderate	-	Moderate
Pyrrhotite (FeS)	-	Weak	Weak	Weak	Moderate
Sphalerite (ZnS)	-	Moderate	Strong	Strong	Strong
Wurtzite (ZnS)	Weak	-	Moderate	Moderate	Moderate
Chalcopyrite ($CuFeS_2$)	Moderate	-	Moderate	-	-
Covellite (CuS)	Moderate	Moderate	Strong	Strong	Weak
Kuramite ($CuSnS_4$)	-	Strong	Strong	Strong	Strong
Renierite $(Cu,Zn)_{11}(Ge,As)_2Fe_4S_{16}$	-	Moderate	Moderate	Strong	Strong

XRD analysis displayed a variation from top to bottom of the core, with a stronger match for sphalerite, covellite (CuS), kuramite (Cu_3SnS_4) and renierite ($(Cu,Zn)_{11}(Ge,As)_2Fe_4S_{16}$) at the deepest part (Table.2). Iron sulfides were present as framboidal structures, flakes and partly dissolved fragments. The variation of morphological features was not observed for sulfides containing copper and zinc. Features thought to be the product of oxidation was detected on the sulfides, especially notable for Cu sulfide (Fig.3d), which was covered in a flaky substance. The Fe sulfide seemed to be partly dissolved with open voids and cracks (Fig.3b).

Based on the changes in spectra after various treatments (Table 1), smectite was the dominating clay mineral group, and was present from 0-20 cm depth. Kaolinite and chlorite as main contributors could be excluded from all depths, but illite could not be excluded from 12, 20 and 25 cm depth. The spectra from 12 and 20 cm depth displayed several similarities, but the spectrum from 25 cm depth differed from these.

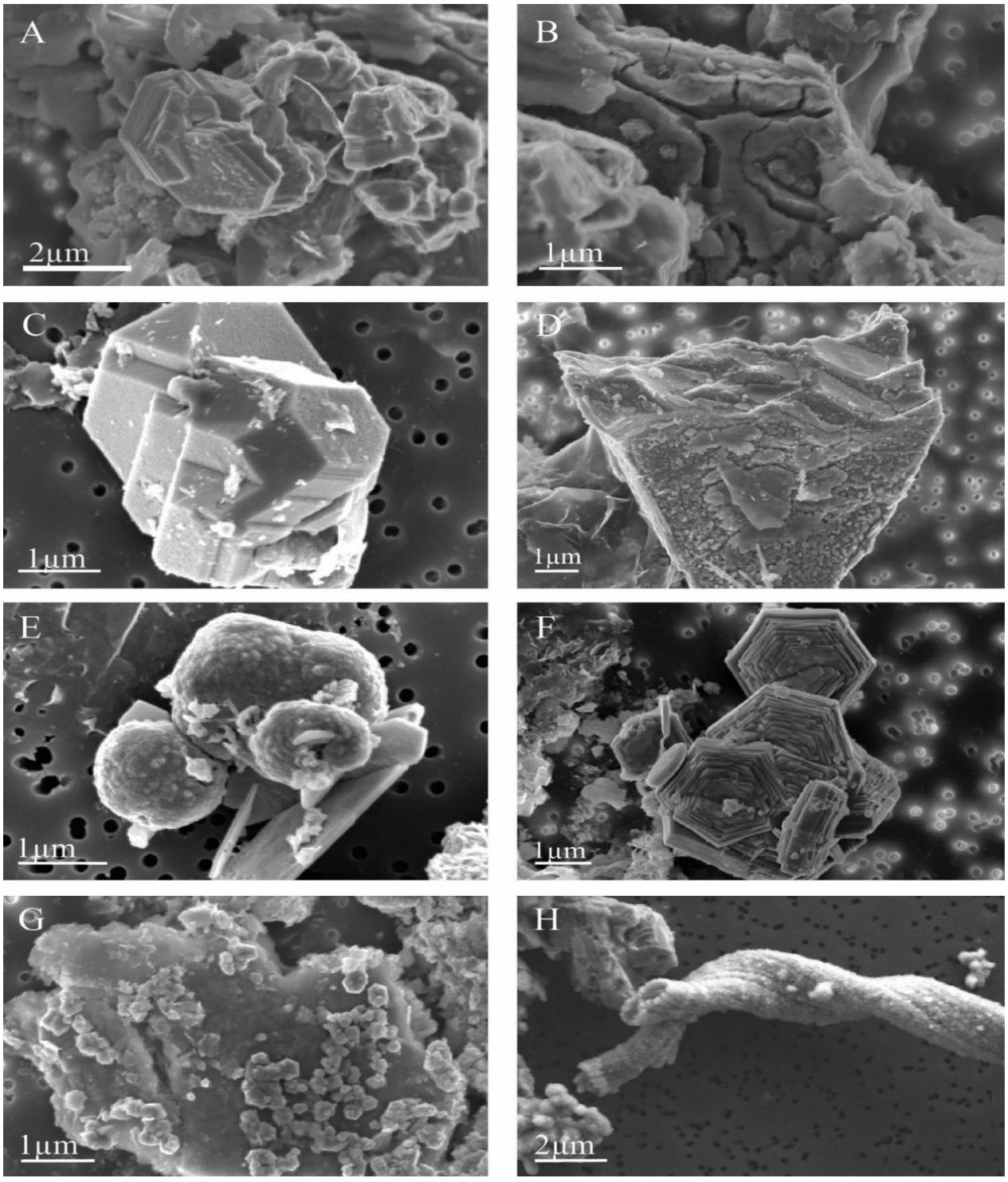

Figure 3: SEM images of sediment grains from different depths of core 1. A: Cu-Fe sulfide covered with a secondary precipitate. B: Fe sulfide with sign of dissolution. C: Zn-Fe sulfide partly covered in secondary precipitate that gives as an uneven surface. D: Cu-Fe sulfide covered by a flaky secondary precipitate. E: Framboidal Fe sulfide (presumably pyrite) surrounding a particle of Ba sulfate. F: Zinc oxide with a wurtzite structure. G: hexagonal particles of Zn oxide covering a Mg-Al silicate. H: Twisted Fe oxyhydroxide stalk.

The presence of oxides was difficult to determine based on regular XRD analysis. At 0-1.5 cm depth, oxides containing a variation of Mn and Fe wereas detected. Based on SEM/EDS analysis, Zn oxide/hydroxide was relatively abundant and detected with various structures and sizes, and showed that a composition of Zn and O was relatively common. Examples of hexagonal flakes and structures analogue to wurtzite indicated that this could be zincite (ZnO) (Nesse, 2012), which was also weakly indicated by XRD analysis at 2, 12 and 20 m depth. The hexagonal zinc oxide covered different minerals, and the observed examples displayed a wide variation in size with no apparent dissolution observed (Fig.3f, g). Twisted stalks, presumably of Fe oxyhydroxide, were observed by SEM (Fig.3h) at different depths of core 1. At 25 cm depth a moderate spectrum match indicates the presence of lepidocrocite (FeO(OH)) at 25 cm depth.

Sulfates (SO_4) with Ba or Ca were detected by SEM-EDS (Fig.3e) and were commonly presented as needles of different thickness. Talc ($Mg_3Si_4O_{10}(OH)_2$) had a weak match with the XRD spectra throughout the core. Different hydrated and none hydrated chlorinated copper phases were indicated by a moderate match in XRD spectra (e.g. nantokite (CuCl)), and some of the chlorinated copper-phases contained lead.

3.2 Solid phase geochemistry

3.2.1 Geochemical composition of the hydrothermal mound material (core 1)

In the mound material SiO_2 (32-41 wt%) was the most abundant oxide, followed by Fe_2O_3 (19-31 wt%) and MgO (13-21 wt%) (Table 3, Fig.4). The SiO_2 content was significantly lower in the surface layer (32 wt%) than in the rest of the core. An opposite trend was observed for Fe_2O_3(T), with the highest value in the surface layer. Significantly lower values were obtained for Na_2O (~2 wt%), Al_2O_3 (~1.5 wt%), CaO (~1 wt%) and K_2O (~0.3 wt%) throughout the core. The total sulfur concentrations decreased downward from 1.7, 2.8 and 7.0 wt% from the top layer to 21-22 cm depth. A similar trend was obtained from sulfidic sulfur with 0.04 wt% in the surface layer, 0.32 wt% at 10-11 cm and 3.03 wt% at 21-22cm depth. The barium content ranged from 2778 to 8257 ppm with the highest value in the deepest part of the core. Zinc increased from 2120 ppm at 0-1.5 cm depth to 8030 ppm at 21-22 cm depth, and the same trend was observed for copper, which increased from 3920 ppm to 6650 ppm. Silver increased from 2.5 ppm to 9 ppm from the top to

bottom of the core. Lead displayed concentrations of 499 ppm at 0-1.5 cm depth, 347 ppm at 10-11 cm depth and 650 ppm at 21-22 cm depth (Table 3, Fig.4) whilst Au displayed the same pattern, with 282, 252 and 449 ppb at the same depths. Cadmium increased from 5.4 at 0-1.5 cm depth to 24.3 ppm at 21-22 cm depth. Arsenic had a concentration of 126 ppm at 0-1.5 and 21-22 cm depth, and 75.9 ppm at 10-11 cm depth. The concentration of organic carbon (TOC) decreased from 0.45 wt% in the surface to 0 wt% at 21-22 cm. Loss of ignition (LoI) was in the range of 11.2-15.7 wt%, with the highest value in the top layer. The slightly low values of total oxides (95.9-97.5 wt%) were likely caused by the content of sulfate minerals, which were detected by SEM/EDS analysis.

3.2.2 Geochemical composition of the background sediment (core 2)

In the background sediment SiO_2 was the most abundant oxide (39-57 wt%), with the lowest concentration at the surface layer, followed by Al_2O_3 (11-15 wt%) (Table 3, Fig.4). CaO varied 17.3- 2.6 wt%, with the highest concentration at the top of the core. Fe_2O_3 had a range off 6-8 wt%, and MgO off 3-6 wt%. Low values were also obtained for Na_2O (~2 wt%) and K_2O (~3 wt%). The MnO content was <1 wt% throughout the core. The total sulfur content was <1 wt%, with the highest content (0.3 wt%) in the surface layer. The concentration of sulfidic sulfur was below detection limit at all depths. The XRF core scan revealed a relative increase of Ba, Zn, Cu and Pb around 20-22 cm depth, which was confirmed by the quantitative analysis (Table 3). Barium ranged from 434-1917, with the lowest value in the deepest part. Copper ranged from 81 to 686 ppm, and Zn from 108 to 274 ppm (Fig.4.), both with the lowest value in the deepest part of the core. Lead (32-236 ppm) and As (22-42 ppm) displayed the same pattern. The concentration of Au varied from below detection limit at 16-17 cm depth to 64 ppb in the surface sample. Concentrations of Cd and Ag were below detection limit at all depths. The TOC content decreased from 0.35 wt% in the surface layer to 0.13 wt% at the deepest part of the core.

Table 3: Geochemical composition at different depths in the two sediment cores.

	Detection limits	Core 1 0-1.5cm	Core 1 10-11cm	Core 1 21-22cm	Core 2 0-1.5cm	Core 2 8-9cm	Core 2 16-17cm	Core 2 21-22cm	Core 2 40-41cm
wt%									
SiO_2	0.01	32.09	41.42	40.71	38.81	55.91	52.59	56.98	49.26
Al_2O_3	0.01	1.63	1.85	0.97	10.85	11.55	13.58	13.53	14.72
Fe_2O_3(T)	0.01	31.32	18.97	22.69	7.95	5.94	6.15	6.84	6.48
MnO	0.001	0.069	0.065	0.10	0.18	0.13	0.15	0.13	0.14
MgO	0.01	12.96	20.7	15.52	4.05	6.02	3.12	4.92	3
CaO	0.01	1.19	0.39	1.64	17.29	4.26	6.74	2.85	7.31
Na_2O	0.01	2.01	2.57	1.54	2.13	2.13	2.14	2.33	2.22
K_2O	0.01	0.36	0.29	0.17	0.8	2.34	3.06	2.55	3.05
TiO_2	0.001	0.047	0.02	0.01	0.71	0.60	0.68	0.7	0.73
P_2O_5	0.01	0.24	0.08	0.02	0.19	0.14	0.11	0.17	0.13
LoI	0.01	15.73	11.19	12.59	16.94	9.95	11.55	9.27	12.5
Total		97.63	97.54	95.85	99.9	98.98	99.87	100.3	99.53
ppm									
Ba	2	3269	2778	8257	1635	1917	479	1359	434
Sr	2	381	209	449	596	253	225	213	236
Y	1	<1	<1	<1	18	20	23	23	24
Sc	1	1	<1	<1	15	11	13	13	14
Zr	2	8	2	<2	89	146	168	167	145
Be	1	<1	<1	<1	1	2	3	2	3
V	5	72	50	21	203	140	141	180	136
As	0.5	126	75.9	126	32.4	29.4	23.8	42.3	22.2
Br	0.5	120	118	76.7	94.4	66.8	67	67.3	66.7
Cr	5	20	<5	<5	98	90	84	100	102
Cs	1	<1	<1	<1	2	3	8	6	10
Co	1	12	19	17	27	23	23	36	20
Ce	3	<3	<3	<3	33	56	83	61	78
Eu	0.2	<0.2	<0.2	<0.2	0.7	0.6	0.9	1.2	0.8
Hf	1	<1	<1	4	4	5	4	5	4
La	0.5	2.9	1.1	1.3	18.2	30.4	42.2	35.2	41.1
Lu	0.05	<0.05	<0.05	<0.05	0.26	0.25	0.29	0.32	0.28
Mo	5	30	<5	<5	<5	<5	<5	<5	<5
Nd	5	<5	<5	<5	28	24	29	38	41
Rb	20	<20	<20	<20	<20	100	160	<20	180
Sb	0.2	3.9	3.5	10.1	0.9	1.2	1.1	1.2	1
Se	3	58	61	110	<3	<3	<3	<3	<3
Sm	0.1	0.3	0.2	0.3	3.2	4.4	5.6	4.9	5.7
Ta	0.5	<0.5	<0.5	<0.5	<0.5	<0.5	<0.5	<0.5	<0.5
Th	0.2	0.9	0.9	<0.2	4	9.1	11.3	8.4	10.8
Tb	0.5	<0.5	<0.5	<0.5	<0.5	<0.5	<0.5	<0.5	<0.5
U	0.5	2.3	<0.5	<0.5	<0.5	1.6	1.3	1.8	<0.5
W	1	<1	<1	<1	<1	<1	<1	<1	<1
Yb	0.2	<0.2	<0.2	<0.2	2.3	2.2	2.6	2.5	2.2
ppb									
Au	2	282	252	449	64	53	<2	63	15
Ir	5	<5	<5	<5	<5	<5	<5	<5	<5
ppm									
Cd	0.5	5.4	6.7	24.3	<0.5	<0.5	<0.5	<0.5	<0.5

	Detection limits	Core 1 0-1.5cm	Core 1 10-11cm	Core 1 21-22cm	Core 2 0-1.5cm	Core 2 8-9cm	Core 2 16-17cm	Core 2 21-22cm	Core 2 40-41cm
Cu	1	3920	4930	6650	686	432	107	378	81
Ni	1	6	6	4	42	43	44	49	48
Zn	1	2120	2570	8030	236	274	145	279	108
Ag	0.3	2.5	3.1	9	<0.3	<0.3	<0.3	<0.3	<0.3
Pb	5	499	347	650	128	74	32	79	23
wt%									
S	0.001	1.68	2.79	7.04	0.34	0.135	0.096	0.118	0.099
Sulfide S	0.01	0.04	0.32	3.03	<0.01	<0.01	<0.01	<0.01	<0.01
TOC		0.45	0.11	0	0.35	0.3	0.13	0.28	0.13

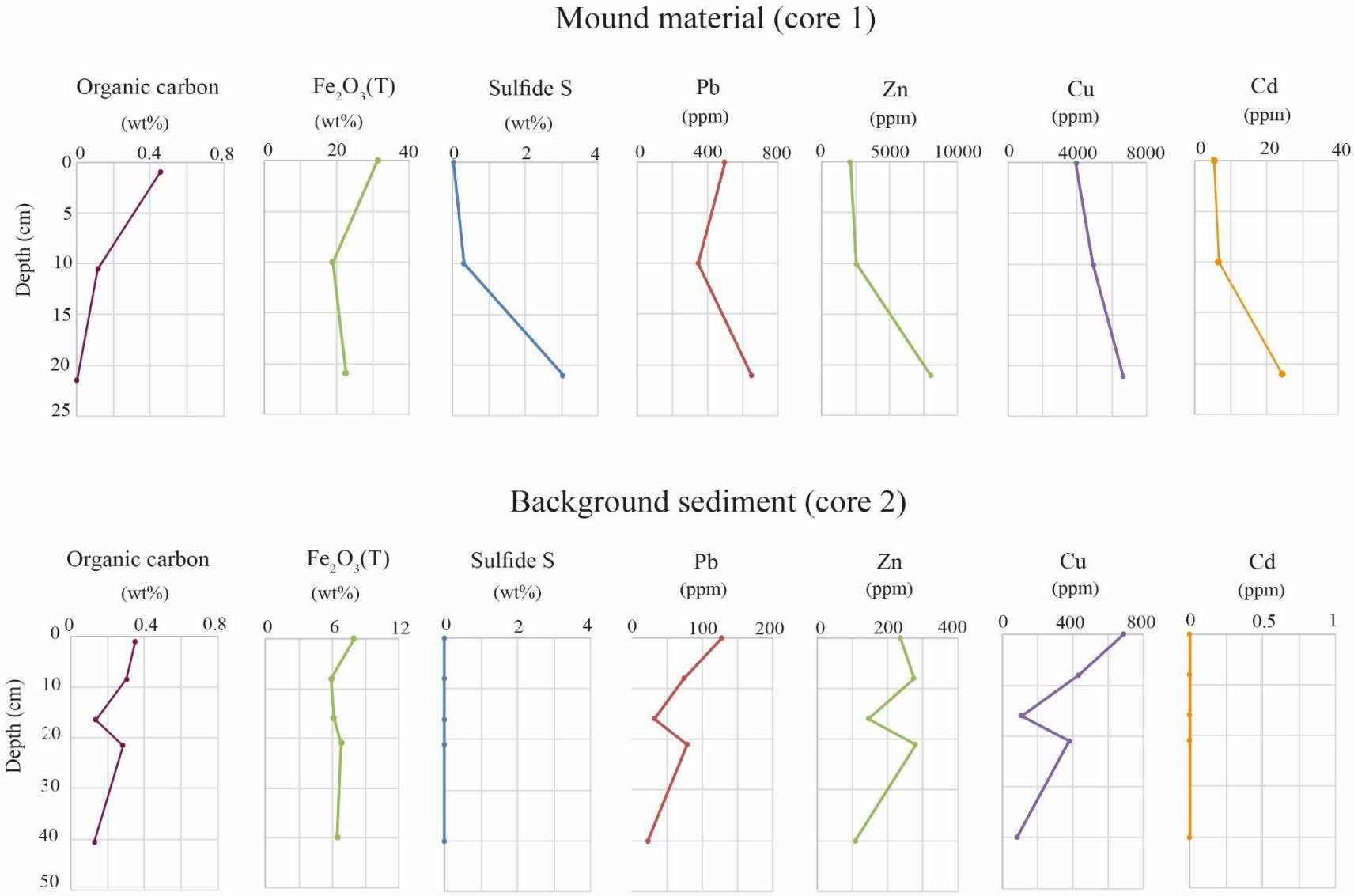

Figure 4: Solid phase geochemistry of the mound material (core 1) and the background sediment (core 2).

3.3 Pore-water geochemistry

3.3.1 Pore-water composition in the mound material (core 1)

In the mound material the pH was close to neutral (7.57-7.65) with the highest value in the surface layer, and the alkalinity was in the range of 1.96-2.76mM (Table 4, Fig.5). The concentration of dissolved O_2 and NO_2 was low, 0.5 and 0.16 µM in the upper part of the core, respectively, and below detection limit in the lower part. Nitrate varied between 6 and 15 µM with the highest concentration in the surface layer. Ammonium ranged from 0.6 to 1.8 µM with the lowest value at the deepest part, showing an opposite pattern from O_2 in the core. Sulfate concentrations were relatively stable between 29-30.2 mM. The Mn concentration varied throughout the core, ranging from 56 to 280 ppb. The Fe concentration decreased with depth, from 3043 in the top layer to 887 ppb in the deepest part. Zinc varied within the core (7-29 ppb) and had the highest concentrations in pore-water from the top layer. Copper displayed the same pattern as Zn, with the highest concentration at the top layer (9 ppb). Cadmium and Pb were detected with concentrations <1 ppb.

3.3.2 Pore-water geochemistry in the background sediment (core 2)

The pore-water from core 2 was slightly basic, ranging from 7.59 to 7.77 (Table 4, Fig.6,), while the alkalinity ranged from 2.3 to 2.6 mM. Oxygen was relatively high throughout the core in the range of 258-287 µM and with the highest concentration in the top of the core. Neither NH_4 nor NO_2 was detected at any depths. Nitrate ranged from 22.33 to 34.22 µM with the lowest value in the upper part. The concentrations of SO_4^{2-} was around 28 mM at all depths. Concentration of Fe ranged between 4-111 ppb, with the highest value in the deepest part of the core. The Zn concentration was between 25-37 ppb throughout the core, whilst Cu ranged from 3 to 10 ppb. The concentration of Pb and Cd were ≤1 ppb. Manganese was detected in bottom water and the pore-water from 45-47 cm depth, with concentrations of 6 and 4.5 ppb, respectively. At other depths, the concentration of Mn was below <1 ppb.

Table 4: Pore-water geochemistry of the mound material (core 1) and the background sediment (core 2). N.a: not analyzed. N.d: not detected. S.W: Bottom seawater

		Core 1, depth (cm)					Core 2, depth (cm)						
		S.W	1-3	7-8	12-14	18-20	S.W	2-4	9-11	18-21	29-31	39-41	45-47
pH		n.a	7.65	7.59	7.57	7.61	n.a	7.59	7.66	7.59	7.66	7.77	7.72
Alk	mM	n.a	2.26	2.76	1.96	2.67	n.a	2.3	2.64	2.44	2.65	n.a	n.a
O2	µM	n.a	0.5	n.d	n.d	n.d	n.a	287	259.5	269	258	261	262
H2S	µM	n.d	n.d	n.d	n.d	n.d	n.a	n.a	n.a	n.a	n.a	n.a	n.a
DIC	mM	2.06	1.93	1.80	1.70	1.97	2.00	2.00	2.10	2.15	2.07	2.03	2.02
NH4	µM	9.85	1.78	1.73	2.18	0.53	n.d	n.d	n.d	n.d	n.d	n.d	n.d
NOt	µM	11.8	14.8	8.9	5.8	12.5	14.1	22.3	24.3	30.9	24.4	34.2	23.0
NO2	µM	n.d	0.16	n.d	n.d	n.d	n.d	n.d	n.d	n.d	n.d	n.d	n.d
NO3	µM	11.8	14.6	8.9	5.8	12.5	14.1	22.3	24.3	30.9	24.4	34.2	23.0
PO4	µM	0.35	0	0.35	0.94	0.29	0.47	1.27	1.46	1.58	1.47	1.3	1.22
Cl	ppm	19849	19822	19869	19721	19899	20008	20326	20294	19856	19577	19677	19903
Br	ppm	62.8	63.3	58.1	61.1	61.3	60.2	59.3	61.1	59.5	60.3	60.6	60.4
SO4	ppm	2877	2971	2858	2863	2861	2855	2823	2830	2850	2835	2836	2844
Na	ppm	10678	10514	10530	10518	10531	10569	10554	10529	10528	10511	10530	10465
Mg	ppm	1282	1237	1239	1243	1247	1263	1239	1237	1238	1239	1235	1227
Ca	ppm	402	394	391	391	392	397	392	391	391	389	389	387
K	ppm	397	397	400	403	396	392	412	411	411	411	413	412
Si	ppb	439	2636	2189	3894	3022	348	2540	2447	2356	2279	2266	2582
Mn	ppb	38.4	189	281	56.2	175.1	5.8	0.68	0.52	0.52	0.37	0.34	4.54
Fe	ppb	9.58	3044	2281	3131	888	28.8	21.4	24.4	22.6	9.30	4.98	112
Sr	ppb	7694	7563	7466	7496	7567	7609	7544	7498	7471	7464	7462	7408
B	ppb	4418	5356	5121	5110	5195	4472	4992	5254	5154	5175	5225	5029
Li	ppb	183	189	181	181	179	181	198	189	193	199	196	201
Ba	ppb	n.d	35.9	35.2	36.9	30.9	n.d	23.1	22.2	21.6	21.7	20.5	20.1
Al	ppb	n.d	n.d	n.d	n.d	n.d	n.d	n.d	n.d	n.d	n.d	n.d	n.d
Ti	ppb	n.d	n.d	n.d	n.d	n.d	n.d	n.d	n.d	n.d	n.d	n.d	0.156
Cr	ppb	n.d	n.d	n.d	n.d	n.d	n.d	n.d	n.d	n.d	n.d	n.d	n.d
Co	ppb	0.39	2.28	8.16	0.52	1.65	1.63	0.21	0.24	0.18	0.28	0.23	0.31
As	ppb	n.a	n.a	n.a	n.a	n.a	n.a	n.a	n.a	n.a	n.a	n.a	n.a

		Core 1, depth (cm)					Core 2, depth (cm)						
		S.W	1-3	7-8	12-14	18-20	S.W	2-4	9-11	18-21	29-31	39-41	45-47
V	ppb	0.89	0.30	0.35	0.22	0.51	0.96	2.67	2.14	2.41	2.26	2.53	2.97
Ni	ppb	15.7	1.06	1.67	0.36	1.97	134	0.77	0.47	0.33	0.25	0.29	0.40
Cu	ppb	9.64	10.25	9.14	2.48	2.76	6.13	2.71	9.85	4.35	4.27	5.00	7.98
Zn	ppb	8.56	29.18	24.18	7.21	18.79	4.61	37.05	26.36	33.41	35.74	24.84	32.91
Cd	ppb	0.05	0.92	0.37	0.10	0.24	0.05	0.08	0.10	0.09	0.09	0.10	0.08834
Pb	ppb	0.02	0.41	0.18	0.09	0.16	0.02	0.09	1.33	0.12	0.07	0.04	0.26
U	ppb	3.03	1.65	2.64	1.28	2.62	3.16	2.99	2.91	2.95	2.95	3.05	3.15

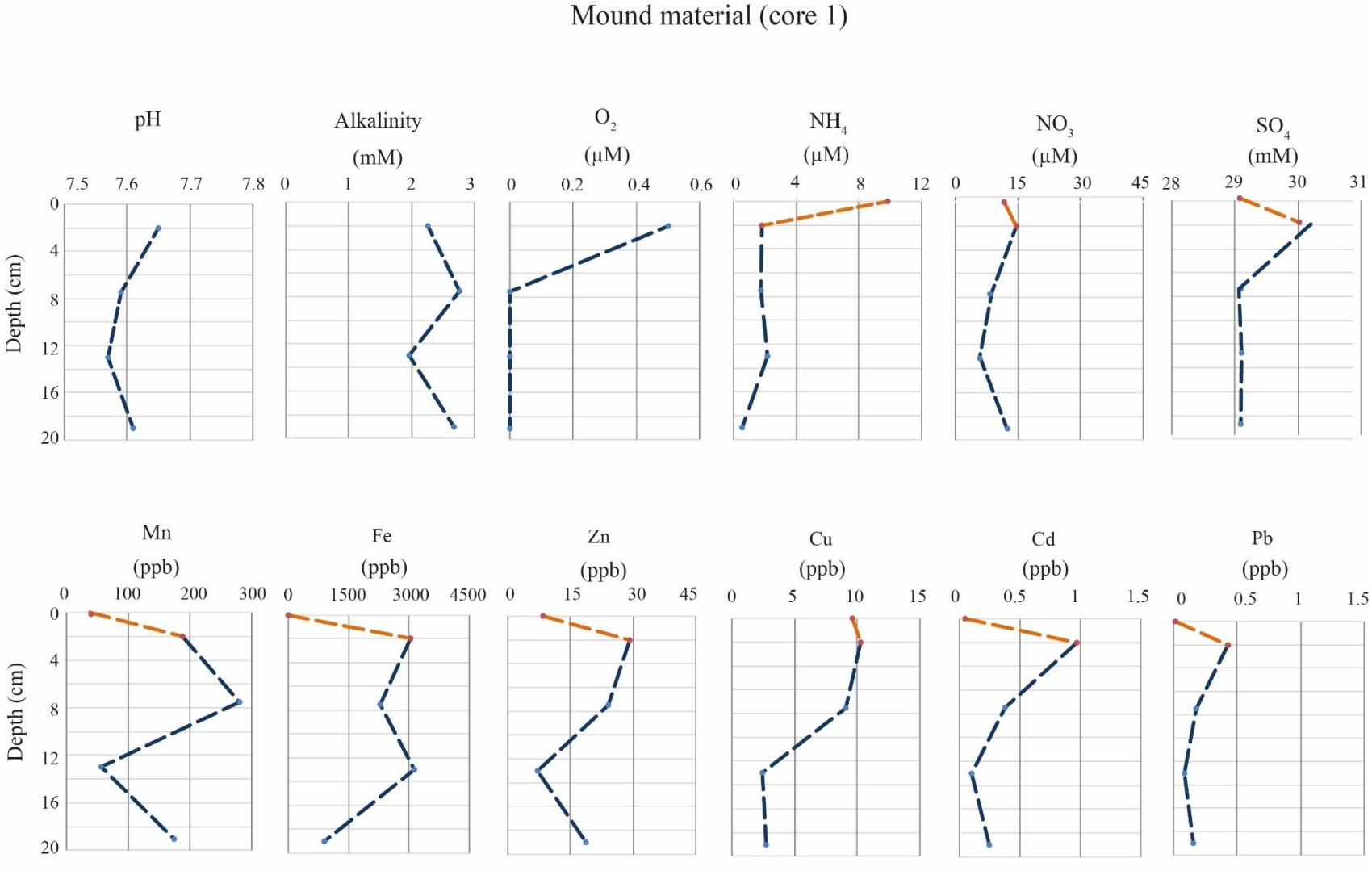

Figure 5: Pore-water geochemistry within the sampled hydrothermal sediment. The values at 0 that are connected to the next value with an orange line represents the bottom seawater sampled within the core liner.

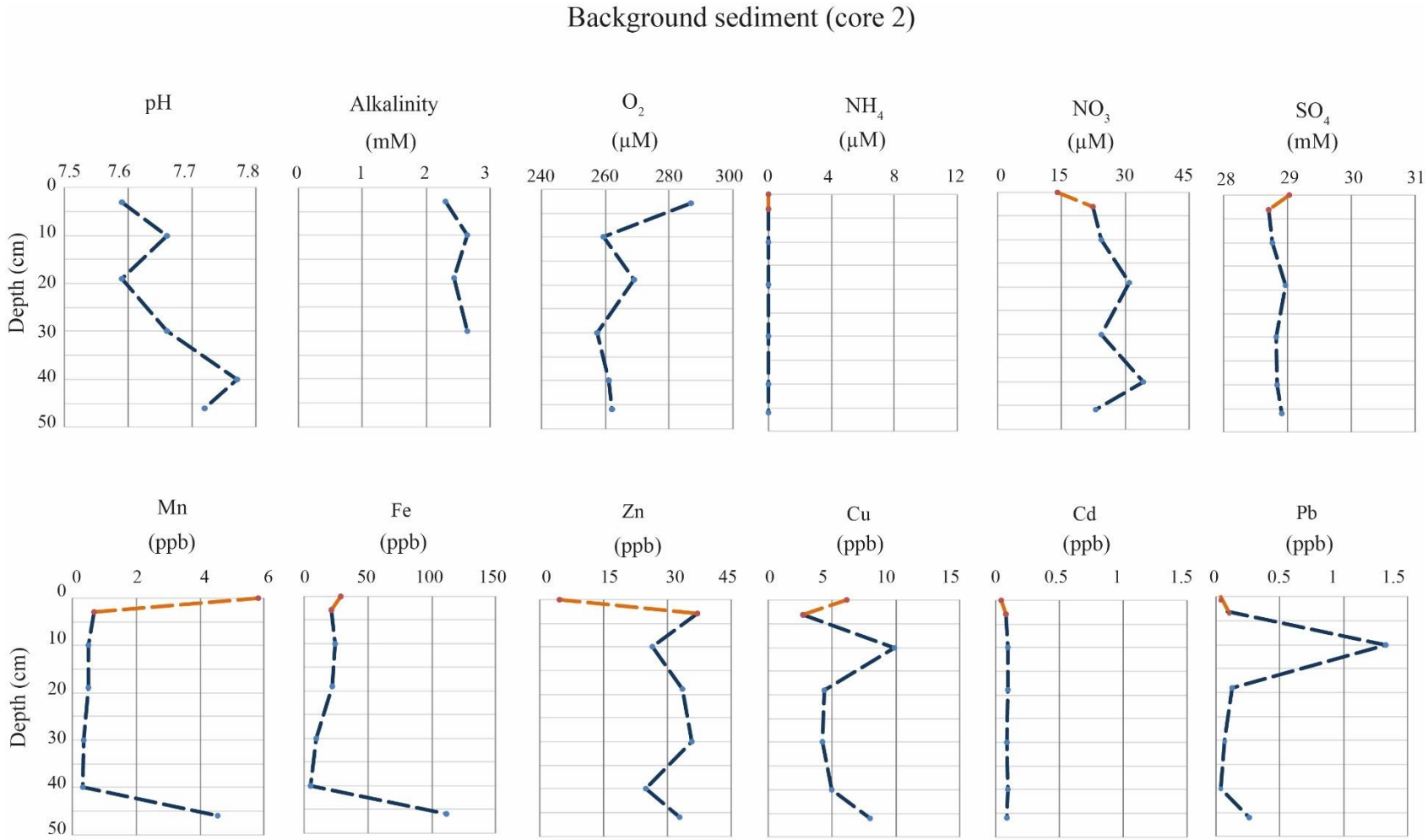

Figure 6: Pore-water geochemistry within the sampled background sediment. The values at 0 cm that are connected to the next value with an orange line represents the bottom seawater sampled within the core liner.

3.4 Microbial community structures

Some main differences between the sediment from the sulfide mound (core 1) and the background sediment (core 2) were detected (Fig.7, Appendix.B). In the mound material there was a higher relative abundance of *Planctomycetia*, *Phycisphaerae, Nitrospira, SJA-4* and *AB16*. Members of *Aquificae* and *OP8_1* were detected in core 1, but not in core 2. In the background sediment (core 1) there was a higher relative abundance of members belonging to the classes *S085, SAR202* and *Acidimicrobiia.* Members of *Thaumarcheaota* were detected in top layers of core 1, and at all depths in core 2. Both cores had a high relative abundance of *Gammaproteobacteria*, *Alphaproteobacteria* and *Deltaproteobacteria.,*

Phylotypes affiliated with *Deltaproteobacteria* are known to be possible SO_4^{2-} reducers (Muyzer and Stams, 2008). *Epsilonproteobacteria* are known to have members that can oxidize sulfur (Muyzer and Stams, 2008), and are important microorganism in sulfidic habitats (Campbell et al., 2006, and refs. therein). Members of *Aquificae* can also oxidize sulfur (Nakagawa, 2004; Nunoura et al. 2008) and together with a class containing Fe reducer (*Deferribacteres,* (Alauzet and Jumas-Bilak, 2014)) and a class associated with Fe oxidation (*Zetaproteobacteria* (Emerson et al., 2007)) the relative abundance of these classes, together with *Epsilonproteobacteria* and *Deltaproteobacteria,* are highlighted in Fig.8. The process of Fe reduction can be performed by other microorganism as well, for example microorganisms affiliated with *Deltaproteobacteria, Firmicutes* and *Crenarchaeota,* as presented in Weber et al., (2006), but due to the higher relative abundance of *Deferribacteres*, this class was chosen to represent this metabolic pathway.

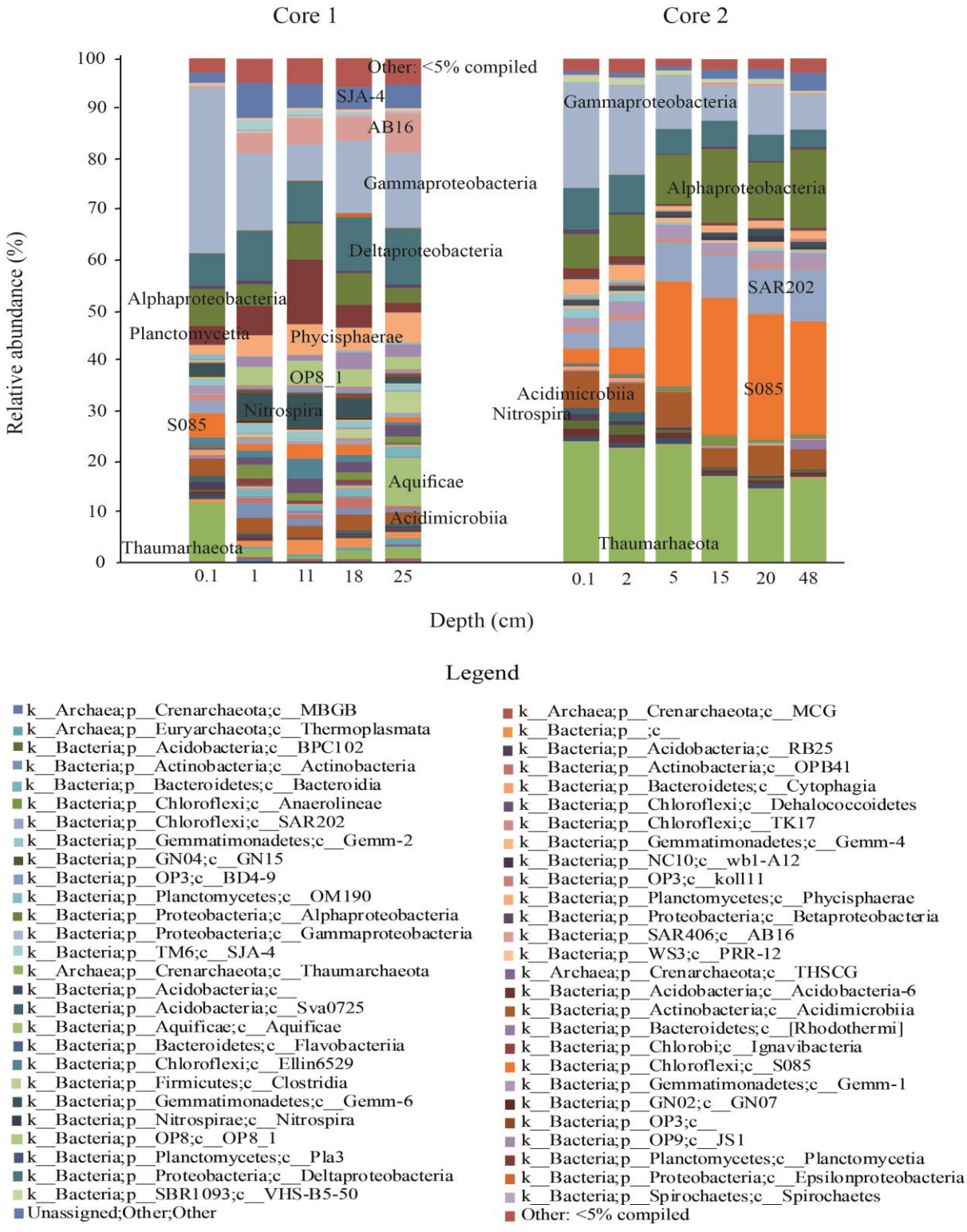

Figure 7: Overview over the microorganisms detected classified down to class level based on the GreenGenes database. When replicates were made the average result is presented. Values are found in Appendix B.

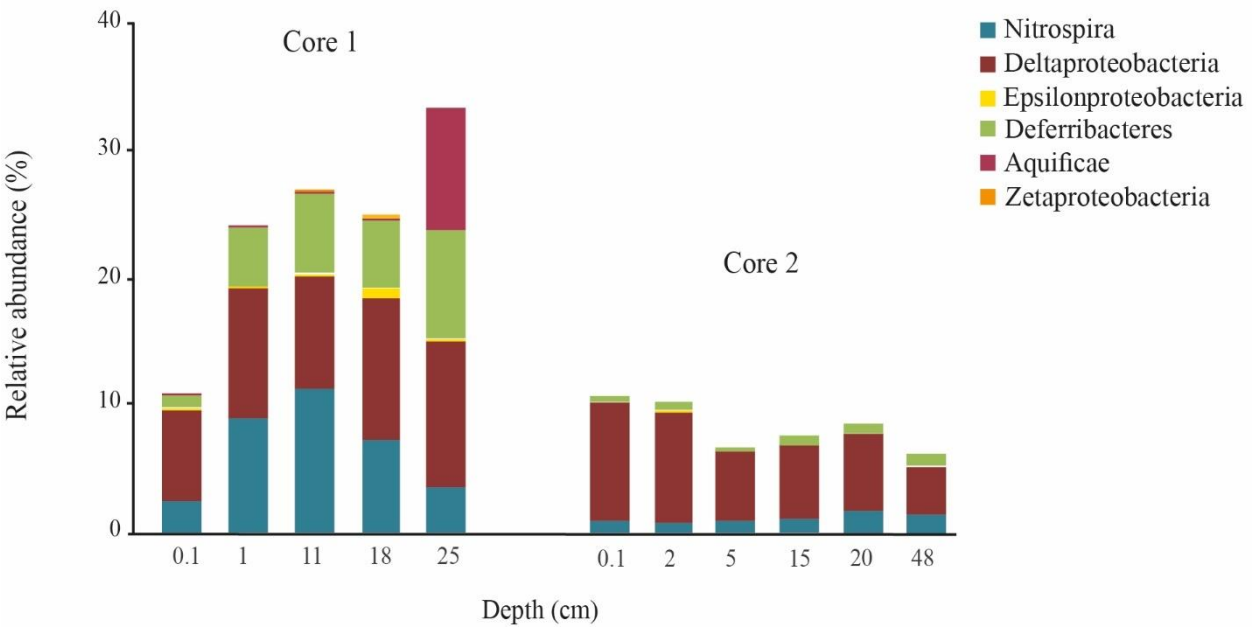

Figure 8: Relative abundance of selected classes from the two cores. Zetaproteobacteria have been included even though the relative abundance is <0.5%.

Members of the class *Nitrospira*, classified down to family *Nitrospiraceae* were detected within both cores. Phylotypes affiliated with *Nitrospira* can be aerobic and anaerobic (Daims, 2014) and further classification show the phylogenetic differences between the two cores. The *Nitrospira* genus, compromised of aerobic NO_2 oxidizers (Daims, 2014), were detected with a relative abundance of 0.3% at 0.1 cm depth and 0.1% at 18 and 25 cm depth in core 1, whereas in core 2, the relative abundance ranged from 0.6-1.2%. *Leptospirillum*, a genus where the species are aerobic and acidophilic Fe^{2+} oxidizer (Daims, 2014) had a relative abundance of 0.4% at 0.1 cm depth and 0.1% at 18 and 25 cm depth in core 1, and ranged from 0-0.5% in core 2. The anaerobic, thermophilic SO_4^{2-} reducing *Thermodesulfovibrio* genus (Daims, 2014) had a relative abundance in range of 0.9-6.6%, with a generally higher relative abundance from 1-18 cm depth, and the highest relative abundance at 11 cm depth in core 1.

Phylotypes affiliated with the phylum *Deferribacteres* were detected in both cores (Silva database) increasing from a relative abundance of 0.9% at 0.1 cm depth to 8.6% at 25 cm depth in core 1. The relative abundance was lower in core 2 with a maximum 0.8% at 48 cm depth. Members of the *Deferribacteres* class are preferentially anaerobes (rarely microaerophilic), neutrophilic,

mesophilic to thermophilic organism which can reduce Fe^{3+}, Mn^{4+}, S^0, Co^{3+} and NO_3^- during degradation of organic matter (e.g. Alauzet and Jumas-Bilak, 2014; Slobodkina, 2009).

Members of *Deltaproteobacteria* were detected with a high relative abundance in core 1, with an average of 9.2%, and a relative abundance as high as 11.1-11.4% in samples from 18-25 cm depth. In core 2 the relative abundance of *Deltaproteobacteria* was 8.0-10.1% at 0.1-2 cm, but the relative abundance displayed a decreasing trend to 3.8% at 48 cm depth. Members associated with the family *Desulfarculaceae* (order: *Desulfarculales*) which is comprised of mesophilic anaerobic SO_4^{2-} reducing bacteria (Kuever et al., 2001) were only detected in core 1. Members of the order *Desulfobacterales* were detected in both cores, but further classification showed that phylotypes affiliated with *Desulfobacteraceae* and *Desulfobulbaceae,* physocrophilic to mesophilic anaerobic SO_4^{2-} reducers (Kuever et.al., 2001), were only found in core 1, whilst members of the none-sulfate reducing *Nitrospinaceae,* a family composed of aerobic NO_2 oxidizers (Kuever et al., 2001), were detected in both cores.

Phylotypes affiliated with *Epsilonproteobacteria* were detected with a relative abundance of 0.1-0.8% in core 1, with the highest abundance at 18 cm depth. In core 2 it was only detected with a low relative abundance (0.1%) at 2 cm depth. Classification down to family level showed the presence of phylotypes affiliated with *Helicobacteraceae* and the genera *Sulfurimonas* and *Sulfurovum* in core 1. *Sulfurimonas* is a mesophilic organism which can oxidize S^0, S^{2-}, $S_2O_3^-$ and H_2 with NO_2^-, NO_3^- and O_2 as electron acceptors (Inagaki, 2003; Takai, 2006), whilst *Sulfuvorum* are able to oxidize S^0 or $S_2O_3^-$ with NO_2^- and NO_3^- as electron acceptors (Inagaki, 2004).

Members of the phylum *Aquificae,* and the order *Aquificales,* were detected with a relative abundance of 0.1-0.2% at 0 to18 cm, and 9.5% at 25 cm depth. *Aquificaceae* was the dominant family within this order, with a relative abundance of 0.1% from 0-18 cm depth and 9.5% at 25 cm depth in the mound material (core 1). Further classification of *Aquificaceae* down to genus showed the presence of *Hydrogenivirga*, a genus with anaerobic to microaerophilic thermophilic organisms, which is capable of oxidizing H_2 or S^0 as an electron donor, and O_2 or NO_3^- as an electron acceptor (Nakagawa, 2004; Nunoura et al. 2008).

Zetaproteobacteria was detected at 11 and 18 cm depth with a relative abundance of 0.1 and 0.3% in core 1, and the only genus within this class is *Mariprofundus,* a mesophilic neutrophilic

microaerophilic iron oxidizer producing stalk like structures (Emerson et al., 2007) previously isolated from iron oxide mats (e.g. Emerson and Moyer, 2002).

4 Discussion

The sediment in the sulfide mound is largely composed of chimney debris and fall out particles formed through precipitation during mixing of emitting hydrothermal fluids and the colder ambient seawater. The primary composition of the sediment in the mound alters with time due to different low-temperature alteration processes, and since many minerals may form both during primary and secondary processes, it is often difficult to determine the origin of the different mineral phases that are identified in the mound material. The microbial communities in the sediment cores can reflect different stages in sediment development, since microorganisms require different growth conditions.

4.1 Sediment formation and weathering

The high Fe_2O_3 content in the mound material (Table 2) reflects different the high content of Fe minerals that precipitates during the high-temperature hydrothermal fluid and seawater mixing. In chimney samples from the Loki's Castle the sulfide assemblage has previously been described as sphalerite, pyrite and pyrrhotite with minor amounts of chalcopyrite (Pedersen et al., 2010a). Covellite has also been detected previously in the Loki's Castle sulfide mound (Økland, pers.com), and the sulfide mineralogy identified in this study (Table 2) is similar of the previous findings. The Cu sulfides kuramite and renierite and the Zn sulfide wurtzite are also seen as likely contributors to the sulfide assemblage in the sediment from the hydrothermal mound in Loki's Castle, and are most likely primary minerals. Mono-sulfides (e.g. covellite and sphalerite) can be produced as a secondary minerals as a result of increased metal concentrations in combination with the production of H_2S (Dvorak et al., 1991; Jong and Parry, 2003; Kaksonen and Puhakka, 2007; Labrenz et al., 2000) during later stage weathering and alteration. Since SO_4^{2-} reducing microorganisms is present throughout core 1 (Fig.7, 8), and SO_4^{2-} reduction produce H_2S, covellite and sphalerite can be microbially induced secondary minerals as well as a primary mineral. Both pyrite and pyrrhotite are presented as parts of a typical black smoker chimney structure together with sphalerite (Haymon, 1983), but the framboidal Fe sulfide (presumably pyrite) detected by SEM-EDS (Fig.3e) can possibly be a secondary mineral, and pyrrhotite can also be a microbially induced secondary mineral as a pre-stage in pyrite formation. Precipitated Fe mono-sulfides, as pyrrhotite, have been shown to form pyrite during a reaction with elemental sulfur at 65°C. The

precipitation of mono-sulfides, and production of elemental sulfur can be catalyzed by microbial activity, and thereby indirectly inducing pyrite formation (Berner, 1970).

Particles with twisted stalk morphologies were detected in the mound material (core 1) by SEM analysis (Fig.3h.), and the stalks are assumed to be composed of poorly crystalline Fe^{3+} oxyhydroxide, as found in other studies (e.g. Picard et al., 2015, and refs. therein). The morphology is linked to members of *Zetaproteobacteria*, which were detected in core 1 (Fig.8), and the only genus affiliated with this class is *Mariprofundus*. *Mariprofundus* has previously been isolated from Fe-mats thought to be precipitated through microbial oxidation of Fe^{2+} derived from Fe-rich fluids, and forms twisted stalks (Emerson et al., 2007). *Mariprofundus* require microaerobic conditions, and the detection in core 1 thereby indicate previously oxygenated conditions in the mound material, and Fe oxyhydroxides are likely formed at these conditions as a product of both abiotical autooxidation and microbial oxidation of Fe^{2+}. *Leptospirillum*, also a group of iron oxidizing microorganisms (Daims, 2014) detected in core 1, have probably contributed to Fe oxyhydroxide formation in the sediment together with *Mariprofundus*. Redox reactions involving Fe can lead to precipitation of different biogenic products from Fe oxidation, for instance goethite and lepidocrocite (Weber et al., 2006, and refs. therein). Goethite (FeO(OH)) was not detected by XRD analysis, but lepidocrocite was detected at 25 cm, and have also been detected in hydrothermal sediment in other studies where it was formed as a product from pyrrhotite oxidation (e.g. Koski et al., 1985). Even though XRD analysis did not give a clear indication of Fe oxides in core 1, the twisted stalks together with the detection of iron oxidizing microorganisms points to the presence of Fe oxides in the mound material, which also can be seen by the rusty color of the sediment (Fig.A-1). A possible explanation for the lack of XRD peaks from Fe oxyhydroxides in the upper part of the core can be due to a poor crystallinity of the phases. In the study by Emerson and Moyer (2002) microbial activity was thought to be the explanation for >50% of the Fe-deposits at five different study sites, and a similar process may explain parts of the Fe detected in core 1.

The Zn oxide detected in core 1 was attached to and partly covered different minerals (Fig.3g), and was most likely precipitated through secondary processes at an early stage in the formation of the deposit, when the minerals were exposed to O_2. The formation of Zn oxide in naturally occurring marine hydrothermal systems has received little attention, but Yamabi and Imai (2002) managed to grow wurtzite structured ZnO in pH from 9-13, by using an aqueous solution with $ZnSO_4$ and

various NH_4^+ salts as complexing agents in a laboratory study. Even though the pH of the pore-water was closer to neutral in the mound material, and the conditions are different, it is possible that the Zn oxide were precipitated when the pH of the pore-water was higher and had a higher O_2 concentration. Since the samples were carbon coated, EDS analysis could not be conclusive regarding the main element composition. Since $ZnCO_3$ has been suggested as a principal control on dissolved Zn in mine waste (e.g. Moncur et al., 2009, and refs. therein) it was tested against the XRD spectra from all depths, but no match was detected. The variety in particle morphology and sizes (e.g. Fig.3f, g), and the lack of dissolution features, can indicate that Zn oxide has a higher stability in an anoxic environment than e.g. Mn oxide, which was not detected with SEM-EDS analysis. Sulfide oxidation during an earlier stage with oxic conditions can have led to oversaturation of Zn in the pore-waters, and thereby a subsequent precipitation of Zn oxide. Since wurtzite was moderately detected in the deepest part of the core, a possible explanation could also be that ZnO is a replacement of the sulfide forming an oxide pseudomorph.

Clay mineral formation by low temperature hydrothermal alteration may also partly explain the high Fe_2O_3 concentration in the mound material, by formation of Fe-rich montmorillonite (McMurtry and Yeh, 1981). The high concentration of MgO in core 1 may be attributed to the formation of Mg-smectite, and possible talc. Talc was weakly indicated by XRD analysis, and could have been formed as Mg-depleted hydrothermal fluids mix with Mg-rich pore-water or seawater at temperatures around 270°C (Koski et al., 1985). Smectite is a group of phyllosilicate minerals species (e.g. montmorillonite, saponite, nontronite) with Si, Al, Fe, Mg, Na, Ca and Li variations in its composition (Odom, 1984). Smectite in hydrothermal settings is commonly formed when seawater Mg^{2+} and (OH^-) are reacting at temperatures <200°C, and it was the clay mineral group detected in the mound material. Most Mg^{2+} uptake at low temperature is a result of seawater composition evolving with depth in the volcanic substrate during restricted circulation, or during low temperature open system alteration of volcanic substrate (Alt, 1995). A dominating clay assemblage could not be identified based spectra change during treatment (see section 2) at 25 cm depth, and this part of the core do not resemble the spectra from 12 and 20 cm, indicating a different origin of the sediment at 25 cm depth. The isolation of the extremophile *Hydrogenivirga* from the outside of a chimney wall in other studies (Nunoura et al. 2008) indicate that the material at 25 cm depth in core 1 may be derived from a higher temperature environment compared to the upper parts of core 1. This part of the collected material may possibly be derived from pieces of a broken

chimney, hosting an active community of extremophiles at the present time. Saponite, a member of the smectite group, have previously found to form in venting chimneys (e.g. Percival and Ames, 1993), but since the change in spectra gave no indication of smectite, saponite is not thought to be present. The different microbial communities detected in the mound material can reflect different stages in the process of sediment formation. *Thermodesulfovibrio,* a genus associated with anaerobic thermophilic SO_4^{2-} reducers (Daims, 2014), were detected continuously in the mound material, and optimum growth of at least four species in this genus is between 55-60°C (Sekiguchi et al., 2008). The detection of *Thermodesulfovibrio* likely reflects a process where higher temperature fluids have been dominant, at a later stage in the sediment formation than *Hydrogenivirga.* The low relative abundance of *Hydrogenivirga* at shallower depths (Fig.7 ,8, 10, Appendix B) indicates that *Hydrogenivirga* and *Thermodesulfovibrio* reflect different processes of sediment formation, as the relative abundance do not follow the same pattern. The presence of microaerobic and mesophilic organisms in core 1 (e.g. *Marifprofundus*) can be explained by increased hydrothermal fluid and seawater mixing, leading to lower temperature and increased O_2 concentration supporting growth of mesophilic and microaerobic microorganism. The detection of the *Nitrospira* genus at 18 and 25 cm depth core 1 can also represent an active community at this stage in mineral formation. Since members of *Nitrospira* genus requires aerobic conditions, *Zetaproteobacteria* requires microaerobic conditions, whilst *Thermodesulfovibrio* is anaerobic, they can reflect short term alternating temperature and O_2 deviations in the fluids. Detection of phylotypes affiliated with the aerobic, ammonia oxidizing archaea *Thaumarchaeota* (Offre et al., 2013) at every depth in core 2 and in the top layers of core 1 (Fig.7) reflects the O_2 content of the two cores, and also the lack of NH_4^+ in core 2 (Fig.5), since NH_4^+ will be oxidized in the presence of O_2 (Konhauser, 2007). The *Nitrospira* genus detected in the top layer of core 1 can also represent parts of an active community.

The extremophiles *Thermodesulfovibrio* and *Aquificae,* were not detected in the background sediment, and this reflects the difference in temperature and substrate in the two sediment cores, as these members are microaerobic to anaerobic thermophilic microorganism, and will not grow under the prevailing conditions found in core 2.The change in microbial communities from top to bottom in the mound material show that several processes have influenced sediment formation, and even though the extremophiles detected might not reflect an active community, they can give more

information about the origin of the sediment and the biogeochemical processes that have been dominant at an earlier stage during formation of the deposit.,

The background sediment (core 2) was assumed to be uninfluenced by hydrothermal activity, consisting mainly of pelagic sediment and glaci-marine sediment derived from the Bear Island Fan (Pedersen et al., 2010a), and do not have the same high Fe_2O_3 and MgO content as the mound material. No mineralogy analysis was performed on the background sediment, but since smectite group clays is commonly formed with a volcanic substrate involved (Alt, 1995), it is not thought to be the dominant clay assemblage in the background sediment. The concentration of Fe_2O_3 and MgO, which can be partly explained by smectite in the mound material, is therefore not expected to be similar in the background sediment as in the mound material. However, a relative increase in Cu, Zn and Pb in the solid phase geochemistry at 21-22 cm depth (Fig.4) is derived from sulfides precipitated as fall out material from the hydrothermal plume during previous active venting.

4.2 Mobilization and immobilization of heavy metals

The decreasing TOC content in the mound material (core 1) show the exhaustion of organic matter with increasing depth in the core. Microorganisms degrading organic matter are dependent on the available electron acceptors in the sediment, and since O_2 is the most energy giving oxidant, O_2 will be used first (Fig.1). The O_2 and NH_4^+ concentration indicate that the mound material was anoxic below 2-8 cm depth (Table 4, Fig.5). The decrease in O_2 concentration was followed by a decrease in NO_3^- and an increase in Mn and Fe concentrations in the pore-water in core 1 (Fig.5), indicating successive use of NO_3^-, and metal oxyhydroxides as terminal electron acceptors in the sediment. Members of the class *Deferribacteres* can reduce chemical species, including NO_3^-, Mn^{4+} and Fe^{3+} (Alauzet and Jumas-Bilak, 2014), and as shown in Fig.9, there is an overall increase in the relative abundance of microorganisms affiliated with this class from top to bottom in the core from the mound. Whether the community data represent active or inactive microorganisms is uncertain, since some of the known members are mesophilic to thermophilic (Alauzet and Jumas-Bilak, 2014; Slobodkina et.al., 2009). However, the detection of a low relative abundance of this class in the background sediment (core 2) as well (Fig.7, 8), may indicate at that members of *Deferribacteres* can grow at lower temperatures, and thereby can represent parts of an active

community in both environments. If they are representing an active community in the mound material (core 1), the increase in relative abundance suggest that there is no exhaustion in the terminal electron acceptors with increasing depth. The alternating pattern between Mn and Fe in the pore-water in core 1 (Fig.9B) can indicate that the more energy yielding MnO reduction (Fig.1) is preferred. The lower MnO concentration at 10-11 cm depth is followed by an increase in pore-water Fe (Fig.9), and a slight increase in solid of phase MnO at the deeper parts of core 1 coincides with an increase in pore-water Mn. The higher concentration of Mn in the top of core 1 can also be due to migration from deeper parts of core, and a higher MnO concentration in the top of the core can reflect oxidation of the upward migrated Mn. If *Deferribacteres* does not represent an active community, the process can still occur by members of other classes associated with this process.

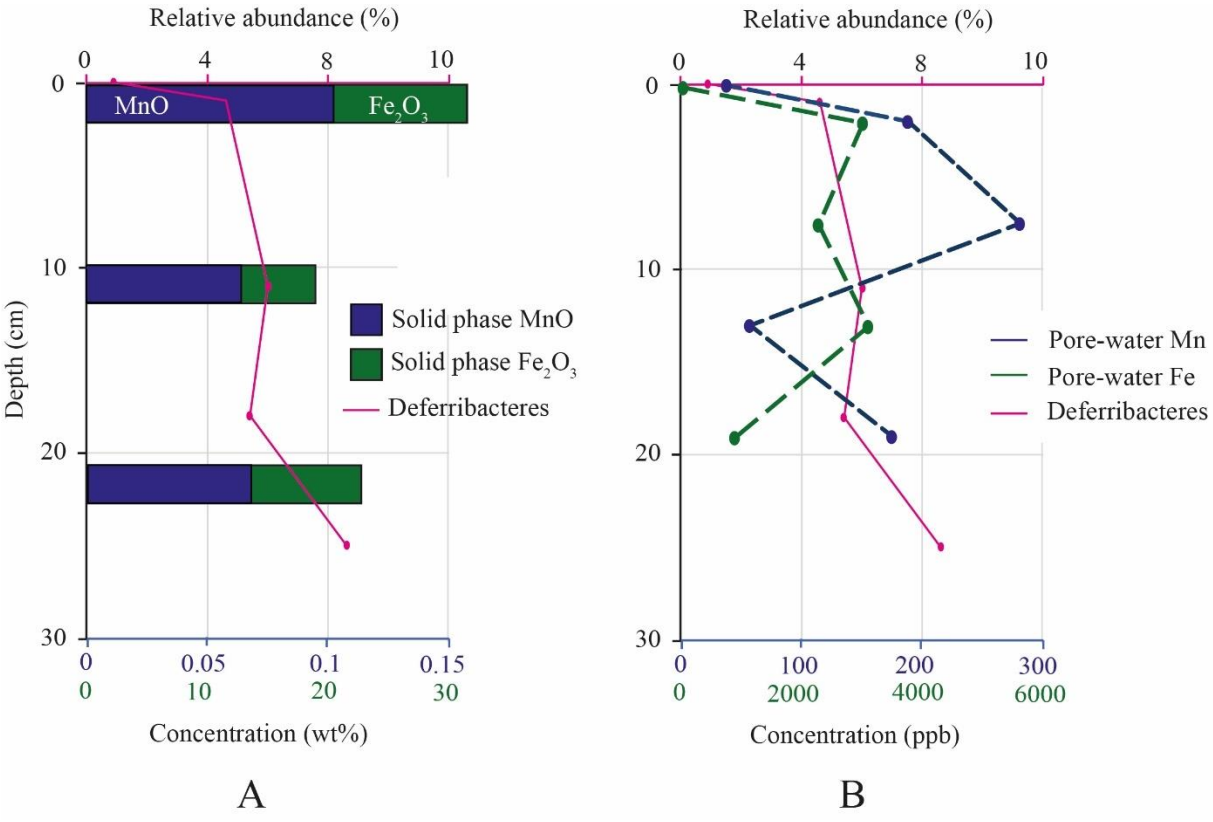

Figure 9: Graphs showing the relative abundance of *Deferribacteres* in core 1 plotted against (A) the solid phase Fe_2O_3 and MnO concentrations, and (B) the pore-water concentrations of Fe and Mn The bars represent 0-1.5, 10-11 and 21-22 cm depth.

Under reducing conditions, the process of oxidation can still occur in sediment can still occur depending on the available of terminal electron acceptors and the microorganism availability to oxidize inorganic substances. Even though anaerobic Fe^{2+} oxidation coupled with NO_3^- reduction have been demonstrated, this process is commonly light dependent. It is thought that light independent oxidation of Fe^{2+} in an anoxic environment occur and contribute to anoxic Fe^{2+} oxidation on a global scale, but this process have been difficult to demonstrate and little is therefore known (Weber et al., 2006, and refs. therein) and this process is not recognized in the mound material.

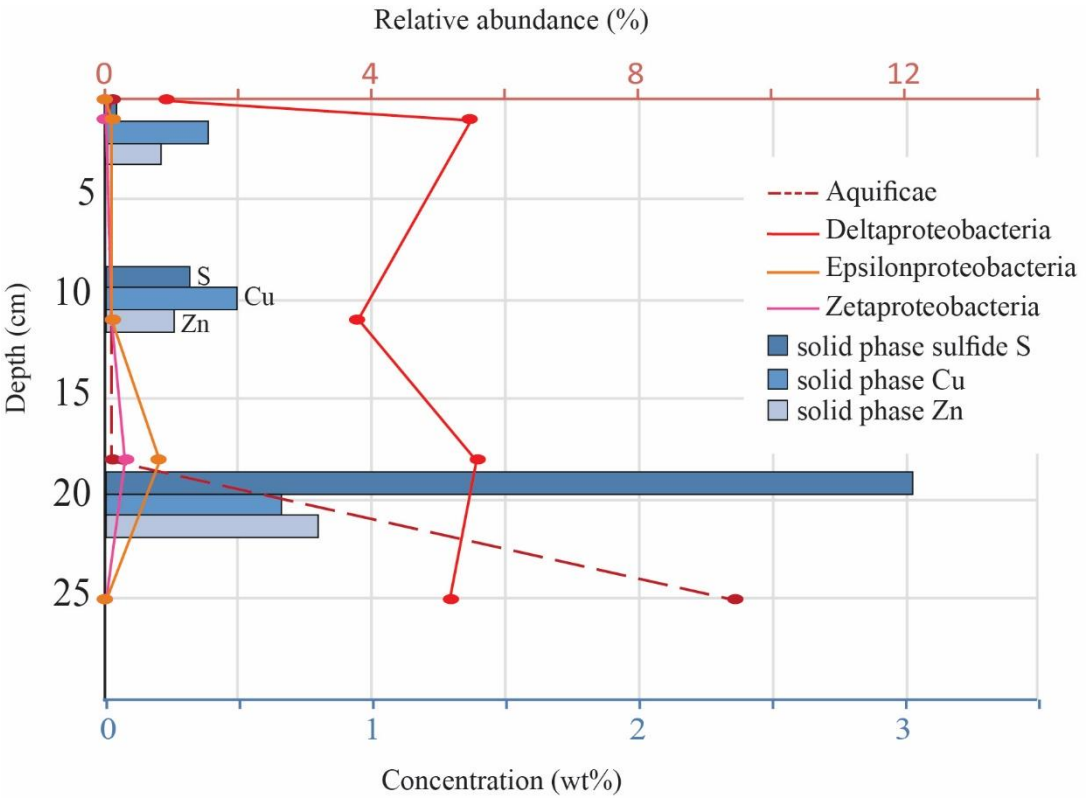

Figure 10: Concentrations of solid phase sulfidic sulfur, Zn and Cu at 0-1.5, 10-11 and 21-22 cm depth in the mound material plotted against the relative abundance of *Aquificae*, *Deltaproteobacteria*, *Epsilonproteobacteria* and *Zetaproteobacteria.* The relative abundance of *Deltaproteobacteria* presented excludes the relative abundance of the non-sulfate reducing *Nitrospinaceae*.

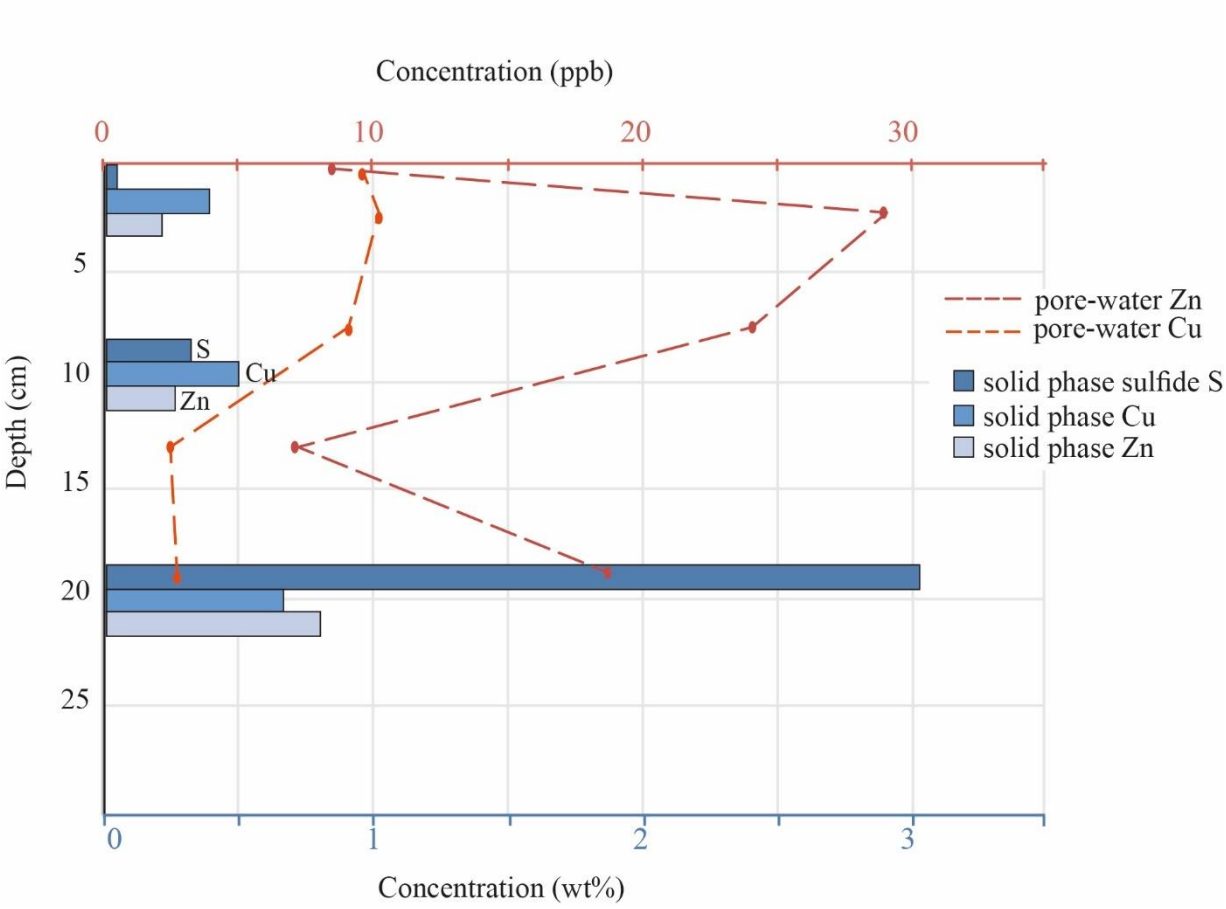

Figure 11: Solid phase sulfidic sulfur, Zn and Cu at 0-1.5, 10-11 and 21-22 cm depth in the hydrothermal sediment, and the pore-water concentrations of Zn and Cu.

However, the lithothrophic sulfide oxidizing microorganisms, increase in relative abundance at 18 cm depth in the mound material (Fig.10). Weathering features were especially notable on Fe sulfides and Cu sulfides (Fig.3a, b, d). Members of the genera *Sulfurimonas* and *Sulfuvorum* can oxidize sulfide and sulfur while reducing NO_3^- (Inagaki, 2003, 2004; Takai, 2006), and likely represent an active community. *Sulfurimonas* can also reduce O_2, and are mesophilic organisms (Inagaki 2003; Takai 2006), and their presence in the mound material may thus also reflect the same stage of sediment formation as *Mariprofundus* and *Nitrospira*. The increase in relative abundance of the sulfur oxidizers coincides with an increase in the solid phase sulfidic sulfur (Fig.10), and can be due to a higher concentration of inorganic substances the microorganisms can utilize for growth. At approximately the same depth, there is a relative increase in dissolved Cu and Zn in the pore-water (Fig.11), which is likely caused by the microbial sulfide oxidation. Sulfide can result in an increase of both SO_4^{2-} and heavy metal concentrations in the pore water is expected

(Eq.1, 3-7), but an increase in SO_4^{2-} was not observed at this depth (Table 4, Fig.5). This is likely attributed to SO_4^{2-} reducers in the, which also display an increase at 18 cm depth (Fig.10). These microorganisms can reduce the SO_4^{2-} produced by sulfide oxidation, and also induce sulfide precipitation by production of H_2S (Dvorak et al., 1991; Jong and Parry, 2003; Kaksonen and Puhakka, 2007).

As seen in the study by Jong and Parry (2003) the removal of heavy metals by SO_4^{2-} reduction will remove Cu from the aquatic phase prior to Zn. This can explain the higher concentration of mobile Zn despite the higher concentration of solid phase Cu in the upper part of core 1 (Fig.10). Trace elements as As and Cd were detected in the mound material, were mainly found to be part of Zn and Cu sulfides by the XRD analysis. Pore-water analysis for As was not performed, so the mobility for this metalloid cannot be determined, but in the study by Jong and Parry (2003) removal of As in the aquatic phase is thought to be controlled by concomitant co-precipitation or adsorption with Zn, Cu, Fe and Ni sulfides. Arsenic has previously been detected in both pyrite (Abraitis et al., 2004) and sphalerite (Labrenz et al., 2000). The same behavior can possibly be attributed to Cd. Previous studies have found Cd as a trace element in e.g. sphalerite (Moncur et al., 2005; Smuda et al., 2007), and it follows the general trend of Zn and Cu in the solid phase (Fig.4). Whether Cd and Pb are found within primary or secondary precipitates is not clear.

Atacamite ($Cu_2Cl(OH)_3$) can form as a secondary product from weathering of sulfides (e.g. Hannington, 1993) but it was not detected in the mound material. The lack of it in the mound material can be due to the prevailing conditions did not favor the formation of this phase, and the chlorinated Cu phases detected by XRD can be attributed to Cu sulfide weathering, with other secondary products than atacamite.

The background sediment (core 2) contained O_2 thorughout the core (Table 4, Fig.6,), and the lack of NH_4^+ indicates that it is oxidized to NO_3^- (e.g. Konhauser 2007). The low TOC content (Fig.4) can explain the aerobic conditions, since a low concentration of organic material, will lead to less use of the terminal electron acceptor available, where O_2 is the first one to be utilized. Even though O_2 is present, other available electron acceptors can possibly be used. The detection of genera affiliated to the class *Deferribacteres* indicates that this can be occurring. Since degradation of organic matter is more energy yielding when reducing O_2, using other electron acceptors is not thought to be the dominant process in the background sediment. Since members of *Deferribacteres*

are anaerobic to microaerophilic (Alauze and Jumas-Bilak, 2014) the detection of this microorganism in core 2 was unexpected. Southam et.al (1995) referenced within (Nordstrom and Southam, 1997) suggests that iron oxidizing organisms can employ nanoenvironments to grow on sulfide mineral surfaces, usually as iron cemented biofilms, and Edwards et.al. (2003, 2004) also used the development of microenvironments as an explanation for the process of oxidation by microaerophilic microorganism in a neutrophilic environment with a relatively high O_2 concentration. A possible explanation for the presence of *Deferribacteres* can be the development of microscale anaerobic environments in the sediment, making the environment more suitable for growth. The concentration of Mn and Fe in the pore-water, which was low in the upper and mid part of the core (Fig.6), would increase during reduction of Mn and Fe oxyhydroxides (Fig.1), but due to the presence of O_2, these elements are thought to be re-oxidized and precipitated. Members of *Deferribacteres* can also reduce NO_3^- (Alauzet and Jumas-Bilak, 2014: Slobodkina, 2009) and since this is a more energy yielding process than reduction of metal oxyhydroxides (Fig.1), it is more likely that this is the dominant process, possibly together with anaerobic to microaerobic small scale environments in the sediment.

Sulfidic sulfur concentrations were below detection limit in the background sediment (core 2), but the relative increase of Zn, Cu and Pb in the solid phase is thought to represent secondary minerals from oxidation of sulfides, which would have been oxidized in the presence of O_2 (Eq.1, 3-7). Only a relative increase in Zn is detected in the pore-water at approximately the same depth, but the concentration of SO_4^{2-} increases slightly in the pore-water at 18-20 cm depth (Fig.6), which can be linked to oxidation of sulfides. An interesting feature was the similar trend observed for Cu and Zn in the solid, and the aquatic phase in core 1 (Fig.4, 5), but this was only observed in the solid phase of core 2 (Fig.4, 6). This can possibly be attributed to the same process as seen during sulfide precipitation (Jong and Parry, 2003), that Cu is removed from the aquatic phase prior to Zn. The alternating pattern may reflect the solubility of the corresponding mineral, and that the mineral containing Zn has a higher solubility than the corresponding Cu mineral in the oxic background sediment.

An increase in pore-water Fe, Mn, Cu, Zn and Pb is seen in the deepest part of core 2 as well (Fig.6), but no relative increase in the mentioned elements was detected in the solid phase by the XRF core scan (data not presented), and quantitative geochemistry analysis were not performed on

the solid material at this depth. The pore-water increase in Zn, Cu and Pb in the deepest part of the core 2 can be attributed to oxidation of sulfide particles, which accumulated in the sediment as hydrothermal fall out material. The pore-water increase of Zn, Cu and Pb can also be caused by possibly double-sampling of the layer affected by hydrothermal activity because of a vertical movement of the ROV's manipulator arm during the procedure.

Comparison of pore-water in the mound material (core 1) and the background sediment (core 2) shows that the concentrations of Zn and Pb are quite similar, with slightly higher Zn and lower Cu concentrations in core 2 (Fig.5, 6). Based on the large difference in solid phase concentrations between the two cores, the heavy metal concentrations in the pore-water from the anoxic mound material were expected to be higher and the concentrations in the oxic background sediment were expected to be lower. The similar pore-water concentrations, even though the solid phase concentrations in the mound material are considerably higher, especially notable for Zn (Fig.4), indicates a relatively higher mobility of the mentioned heavy metals in an oxygenated environment. These unexpected results are likely related to the difference in the microbial community in the two sediment cores, and especially the lack of SO_4^{2-} reducers in the oxic background sediment. The mobility of heavy metals is dependent on precipitation of secondary minerals, and in core 1 the mobility is thought to be controlled by sulfide precipitation. The detected SO_4^{2-} reducers in the mound material (core 1) demonstrate how microbial activity may influence the mobility of the heavy metals in the pore-water. Sulfate reducing microorganisms produce H_2S, that is necessary for sulfide precipitation. Precipitation of sulfides is thereby directly dependent on the presence of SO_4^{2-} reducing microorganisms. The lack of SO_4^{2-} reducing microorganisms in core 2 show that sulfide precipitation is not a dominant process in this sediment, and the mobility of the heavy metals is controlled by other processes. Comparison of the relative mobility of heavy metals in the two cores, show that microbially induced sulfide precipitation is more efficient in removing dissolved heavy metals than processes dominating in oxic sediment.

4.3 Implications for future deep-sea mining

The mobilization of heavy metals through generation of AMD do not seem as a likely scenario during seafloor mining based on finding in this study, however, other processes can mobilize heavy

metals in the marine environment. The biogeochemical processes dominating the two sediment cores show that the sediment exposed to oxic conditions can have less capacity to immobilize heavy metals dissolved in the pore-water. Grinded and reworked sulfidic ore material will, during the planned mining operation, be exposed to oxic conditions at the seafloor. The process will lead to oxidation and production of metal hydroxides (Eq.1-9), and possibly increase the metal concentrations in the surrounding waters. Sulfides in the unconsolidated material moved prior to exploitation will likely go through the same oxidation process, and as material will be dispersed evenly on seafloor, it will influence the sediment composition. Even though the sedimentation is calculated to not surpass the natural sedimentation rate (Nautilus Mineral Inc, 2016), the substrate will differ from that naturally deposited, and likely have an effect on the local marine biota. By using the oxic core as an analog to the processes occurring during the re-deposition of sulfidic material, re-deposition will likely increase the metal concentration in the surrounding waters, as the heavy metals are considered to be relatively more mobile in this environment. The oxic environment does not support the growth of SO_4^{2-} reducing microorganisms, and thereby the precipitation of metal sulfides induced by microbial activity will not occur. The material that is lost on the seafloor and not retrieved (Nautilus Mineral Inc., 2016) will continue to oxidize as long as it is exposed at the seafloor, and possibly also after burial, but then due to a different set of processes.

During the planned mining operations, already oxidized material will be pumped back from the dewatering process on land, and be evenly dispersed across the seafloor (Nautilus Mineral Inc, 2016). The already oxidized material will abruptly increase the heavy metal concentration in the surrounding water immediately after disposal. Immobilization of heavy metals by sulfide precipitation will not occur in this setting, and adsorption or concomitant precipitation of oxides or other minerals are likely controlling the immobilization of the heavy metals, a process thought to be less efficient than sulfide precipitation.

5 Conclusions

The mound material (core 1) has gone through several changes in conditions before reaching current state, which is reflected in the mineralogy and the microbial communities detected. Temperature and O_2 concentrations have probably fluctuated during the sediment formation, leading to precipitation of various sulfides, oxides and clay minerals. In core 2 the sediment is mainly derived from pelagic and glaci-marine sediment, with a layer of hydrothermal fall out material at 21-22 cm depth.

In the two sediment cores different biogeochemical processes are dominating, which is controlled by the primary minerals. The background sediment was oxic and the mound material was anoxic, and the differences are reflected by the high relative abundance of SO_4^{2-} reducers in the anoxic mound material. In the anoxic mound material, the microbial oxidation of sulfides and reduction of oxides and SO_4^{2-} is thought to be an active process, resulting in precipitation of secondary sulfides. Previously precipitated oxides in the mound material are considered unstable at present conditions, and they can contain various trace elements that can be released to the pore-water. The heavy metals released are immobilized through microbiologically induced sulfide precipitation. In the oxic background sediment, oxidation of sulfides and precipitation of oxides is likely dominant processes, and the sulfides can be oxidized by biotical and abiotical processes.

Even though the implications on on-land mining cannot be directly transferred to the marine environment, an analog to the process can be derived from comparing the two sediment cores analyzed in this study. By comparing the two different sediment, the similar values of Zn, Pb and partly Cu in the pore-water despite the large deviation in concentrations in the solid phase, show that these metals can have a lower mobility in the anoxic compared to oxic environment, and it is thought to be related to the presence of SO_4^{2-} reducing microorganisms, which catalyze sulfide precipitation. As seen from the differences in the environment of the two cores, the background sediment does not support the growth of SO_4^{2-} reducing microorganisms, and thereby microbially induced sulfide precipitation will not occur, and adsorption or concomitant precipitation to oxides or other minerals must be controlling the immobilization of the heavy metals in this environment.

The findings of this study can be related to future seafloor mining, as the redistribution of sulfidic material in an oxic environment can increase the metal concentrations in the surrounding water, an

environment not supportive of microorganisms that can catalyze sulfide precipitation. Immobilization is therefore dependent of adsorption/coprecipitation to oxides, a process that seems to be less efficient, and can possibly lead to an increase in heavy metals in the aquatic phase. An increase of the heavy metal in the surrounding waters can have unexpected short and long term consequences, both in local and in larger areas, and further biogeochemical studies is necessary to increase the knowledge regarding environmental impacts regarding future deep-sea mining operations.

6 Further work

There are still many unanswered questions related to the biogeochemical processes occurring in hydrothermal mound sediment, and also to the controlling factors on the mobility of heavy metals in the oxic sediment. Further knowledge regarding these processes can increase the knowledge of environmental impacts of deep-sea mining. As seen in this study, further work including biogeochemical studies can be useful in determining the behavior of heavy metals that are remobilized during the mining operations, and can possibly be used to evaluate the possible environmental impacts of deep-sea mining operations.

In direct relation to this study, further microbial analysis in terms of differencing active and inactive communities could increase the knowledge regarding the role of microbial activity in the process of immobilizing the metals. It could also be interesting to look further into the mineralogy in the mound material to determine if they are mainly present in primary or secondary precipitates, and also investigate the same processes in the background sediment. If possible, a definition of what oxides and other minerals that are present could be useful in the background sediment, as the solubility could be used to further determine secondary precipitation processes influencing the process of immobilization. Also, the formation of ZnO in hydrothermal systems could be interesting to study, as little research has been done on this so far, and it could be useful when investigating mobility of Zn.

7 Reference list

Abraitis, P.K., Pattrick, R.A.D., Vaughan, D.J., 2004. Variations in the compositional, textural and electrical properties of natural pyrite: a review. Int. J. Miner. Process. 74, 41–59.

Actlabs-Lithium Metaborate/Tetraborate Fusion-ICP-Geochemistry / Assay | Actlabs [WWW Document], <http://www.actlabs.com/page.aspx?page=514&app=226&cat1=549&tp=12&lk=no&menu=64> (accessed 10.28.16).

Actlabs-Lithogeochemistry-Geochemistry | Actlabs [WWW Document], <http://www.actlabs.com/page.aspx?menu=74&app=244&cat1=595&tp=2&lk=no> (accessed 11.24.16).

Actlabs-Total Digestion-ICP-Geochemistry / Assay | Actlabs [WWW Document], <http://www.actlabs.com/page.aspx?page=848&app=226&cat1=549&tp=12&lk=no&menu=64> (accessed 10.28.16).

Actlabs-Sulphide-Geochemistry / Assay | Actlabs [WWW Document], <http://www.actlabs.com/page.aspx?page=733&app=226&cat1=549&tp=12&lk=no&menu=64> (accessed 10.28.16).

Alauzet, C., Jumak-Bilak., 2014. The Phylum Deferribacteres and the Genus Caldhithrix, in: Rosenberg, E., DeLong, E.F., Lory, S., Stackebrandt, E., Thompson, F. (Eds.), The Prokaryotes. Springer Berlin Heidelberg, Berlin, Heidelberg, pp. 595 – 611.

Alt, J.C., 1995. Subseafloor Processes in Mid-Ocean Ridge Hydrothennal Systems. Seafloor Hydrothermal Syst. Phys. Chem. Biol. Geol. Interact. 85–114.

Baumberger, T., Früh-Green, G.L., Dini, A., Boschi, C., van Zuilen, K., Thorseth, I.H., Pedersen, R.B., 2016a. Constraints on the sedimentary input into the Loki's Castle hydrothermal system (AMOR) from B isotope data. Chem. Geol. 443, 111–120.

Baumberger, T., Früh-Green, G.L., Thorseth, I.H., Lilley, M.D., Hamelin, C., Bernasconi, S.M., Okland, I.E., Pedersen, R.B., 2016. Fluid composition of the sediment-influenced Loki's Castle vent field at the ultra-slow spreading Arctic Mid-Ocean Ridge. Geochim. Cosmochim. Acta 187, 156–178.

Berner, R.A., 1970. Sedimentary pyrite formation. Am. J. Sci. 268, 1–23.

Brazelton, W.J., Ludwig, K.A., Sogin, M.L., Andreishcheva, E.N., Kelley, D.S., Shen, C.-C., Edwards, R.L., Baross, J.A., 2010. Archaea and bacteria with surprising microdiversity show shifts in dominance over 1,000-year time scales in hydrothermal chimneys. Proc. Natl. Acad. Sci. 107, 1612–1617.

Campbell, B.J., Engel, A.S., Porter, M.L., Takai, K., 2006. The versatile ε-proteobacteria: key players in sulphidic habitats. Nat. Rev. Microbiol. 4, 458–468

Carr, R.S., Nipper, M., Plumlee, G.S., 2003. Survey of Marine Contamination from Mining-Related Activities on Marinduque Island, Philippines: Porewater Toxicity and Chemistry. Aquat. Ecosyst. Health Manag. 6, 369–379.

Crundwell, F.K., Verbaan, B., 1987. Kinetics and mechanisms of the non-oxidative dissolution of sphalerite (zinc sulphide). Hydrometallurgy 17, 369–384.

Daims, H. The Family Nitrospira, in: Rosenberg, E., DeLong, E.F., Lory, S., Stackebrandt, E., Thompson, F. (Eds.), The Prokaryotes. Springer Berlin Heidelberg, Berlin, Heidelberg, pp. 733-749.

Dahle, H., Økland, I., Thorseth, I.H., Pederesen, R.B., Steen, I.H., 2015. Energy landscapes shape microbial communities in hydrothermal systems on the Arctic Mid-Ocean Ridge. ISME J. 9, 1593–1606.

Dold, B., 2014. Submarine Tailings Disposal (STD)—A Review. Minerals 4, 642–666.

Dvorak, D.H., Hedin, R. s., Edenborn, H.M., Mcintire, P.E., 1991. Treatment of metal-contaminated water using bacterial sulfate reduction: results from pilot-scale reactors. J. Am. Soc. Min. Reclam. 1991, 109–122.

Edwards, K.J., Bach, W., McCollom, T.M., Rogers, D.R., 2004. Neutrophilic Iron-Oxidizing Bacteria in the Ocean: Their Habitats, Diversity, and Roles in Mineral Deposition, Rock Alteration, and Biomass Production in the Deep-Sea. Geomicrobiol. J. 21, 393–404.

Edwards, K.J., McCollom, T.M., Konishi, H., Buseck, P.R., 2003. Seafloor bioalteration of sulfide minerals: results from in situ incubation studies. Geochim. Cosmochim. Acta 67, 2843–2856.

Ehrlich, H.L., 1999. Microbes as Geologic Agents: Their Role in Mineral Formation. Geomicrobiol. J. 16, 135–153.

Emerson, D., Moyer, C.L., 2002. Neutrophilic Fe-Oxidizing Bacteria Are Abundant at the Loihi Seamount Hydrothermal Vents and Play a Major Role in Fe Oxide Deposition. Appl. Environ. Microbiol. 68, 3085–3093.

Emerson, D., Rentz, J.A., Lilburn, T.G., Davis, R.E., Aldrich, H., Chan, C., Moyer, C.L., 2007. A Novel Lineage of Proteobacteria Involved in Formation of Marine Fe-Oxidizing Microbial Mat Communities. PLoS ONE 2, e667.

Hannington, M., 1993. The formation of atacamite during weathering of sulfides on the modern seafloor. The Canadian Mineralogist 31, 945-956.

Haymon, R.M., 1983. Growth history of hydrothermal black smoker chimneys. Nature 301, 695–698.

Hoagland, P., Beaulieu, S., Tivey, M.A., Eggert, R.G., German, C., Glowka, L., Lin, J., 2010. Deep-sea mining of seafloor massive sulfides. Mar. Policy 34, 728–732.

Hoffman, E.L., 1991. Instrumental neutron activation in geoanalysis. J. Geochem. Explor. 44, 297–319.

Inagaki, F., 2004. Sulfurovum lithotrophicum gen. nov., sp. nov., a novel sulfur-oxidizing chemolithoautotroph within the -Proteobacteria isolated from Okinawa Trough hydrothermal sediments. Int. J. Syst. Evol. Microbiol. 54, 1477–1482.

Inagaki, F., 2003. Sulfurimonas autotrophica gen. nov., sp. nov., a novel sulfur-oxidizing -proteobacterium isolated from hydrothermal sediments in the Mid-Okinawa Trough. Int. J. Syst. Evol. Microbiol. 53, 1801–1805.

Janzen, M.P., Nicholson, R.V., Scharer, J.M., 2000. Pyrrhotite reaction kinetics: reaction rates for oxidation by oxygen, ferric iron, and for nonoxidative dissolution. Geochim. Cosmochim. Acta 64, 1511–1522.

Jong, T., Parry, D.L., 2003. Removal of sulfate and heavy metals by sulfate reducing bacteria in short-term bench scale upflow anaerobic packed bed reactor runs. Water Res. 37, 3379–3389.

Kaksonen, A.H., Puhakka, J.A., 2007. Sulfate Reduction Based Bioprocesses for the Treatment of Acid Mine Drainage and the Recovery of Metals. Eng. Life Sci. 7, 541–564.

Konhauser, K., 2007. Introduction to geomicrobiology. Blackwell, Malden, Mass.

Koski, R.A., Lonsdale, P.F., Shanks, W.C., Berndt, M.E., Howe, S.S., 1985. Mineralogy and geochemistry of a sediment-hosted hydrothermal sulfide deposit from the Southern Trough of Guaymas Basin, Gulf of California. J. Geophys. Res. Solid Earth 90, 6695–6707.

Kuever, J., Rainey. F.A., Widdel. F., Order III. Desulfobacterales, in: D.R., Castenholz, R.W., Garrity, G.M. (Eds.), 2001. Bergey's manual of systematic bacteriology, 2nd ed. ed. Springer, New York, pp. 959-1005

Labrenz, M., Druschel, G.K., Thomsen -Ebert, T., Gilbert, B., Welch, S.A., Kemner, K.M., Logan, G.A., Summons, R.E., 2000. Formation of Sphalerite (ZnS) Deposits in Natural Biofilms of Sulfate-Reducing Bacteria. Science 290, 1742–1744.

Lindsay, M.B.J., Condon, P.D., Jambor, J.L., Lear, K.G., Blowes, D.W., Ptacek, C.J., 2009. Mineralogical, geochemical, and microbial investigation of a sulfide-rich tailings deposit characterized by neutral drainage. Appl. Geochem. 24, 2212–2221.

Lindsay, M.B.J., Moncur, M.C., Bain, J.G., Jambor, J.L., Ptacek, C.J., Blowes, D.W., 2015. Geochemical and mineralogical aspects of sulfide mine tailings. Appl. Geochem. 57, 157–177.

McMurtry, G.M., Yeh, H.-W., 1981. Hydrothermal clay mineral formation of East Pacific rise and Bauer Basin sediments. Chem. Geol. 32, 189–205.

Moncur, M.C., Jambor, J.L., Ptacek, C.J., Blowes, D.W., 2009. Mine drainage from the weathering of sulfide minerals and magnetite. Appl. Geochem. 24, 2362–2373.

Moncur, M.C., Ptacek, C.J., Blowes, D.W., Jambor, J.L., 2005. Release, transport and attenuation of metals from an old tailings impoundment. Appl. Geochem. 20, 639–659.

Moses, C.O., Herman, J.S., 1991. Pyrite oxidation at circumneutral pH. Geochim. Cosmochim. Acta 55, 471–482.

Moses, C.O., Kirk Nordstrom, D., Herman, J.S., Mills, A.L., 1987. Aqueous pyrite oxidation by dissolved oxygen and by ferric iron. Geochim. Cosmochim. Acta 51, 1561–1571.

Multi EA 4000, Analytik Jena AG.pdf [WWW Document], n.d. URL <http://www.analytikjenaromania.ro/sites/default/files/td_multi_EA_4000_en_0.pdf> (accessed 12.1.16).

Muyzer, G., Stams, A.J.M., 2008. The ecology and biotechnology of sulphate-reducing bacteria. Nat. Rev. Microbiol.

Nakagawa, S., 2004. Hydrogenivirga caldilitoris gen. nov., sp. nov., a novel extremely thermophilic, hydrogen- and sulfur-oxidizing bacterium from a coastal hydrothermal field. Int. J. Syst. Evol. Microbiol. 54, 2079–2084.

Nautilus Mineral Inc, 2016. Environmental Impact Statement-Main Report. [WWW Document] <http://www.nautilusminerals.com/irm/content/pdf/environment-reports/Environmental%20Impact%20Statement%20-%20Main%20Report.pdf> (accessed 12.07.16)

Nesse, W. D., 2012. Introduction to Mineralogy. 2 ed. Oxford University press, New York.

Nordstrom, D.K., 1982. Aqueous Pyrite Oxidation and the ConsEquent Formation of Secondary Iron Minerals, in: Acid Sulfate Weathering, SSSA Special Publication. Soil Science Society of America, Madison, WI, pp. 37–56.

Nordstrom, D.K., 2011. Hydrogeochemical processes governing the origin, transport and fate of major and trace elements from mine wastes and mineralized rock to surface waters. Appl. Geochem. 26, 1777–1791.

Nordstrom, K., D., Southam, G., 1997. Geomicrobiology of sulfide mineral oxidation, in: Banfield, J.F., Nealson, K.H. (Eds)., Geomicrobiology: Interactions between Microbes and Minerals Rosenberg. Reviews in Mineralogy, Min. Soc. Am, Washington, pp. 361-390.

Nunoura, T., Miyazaki, M., Suzuki, Y., Takai, K., Horikoshi, K., 2008a. Hydrogenivirga okinawensis sp. nov., a thermophilic sulfur-oxidizing chemolithoautotroph isolated from a deep-sea hydrothermal field, Southern Okinawa Trough. Int. J. Syst. Evol. Microbiol. 58, 676–681.

Odom, I.E., 1984. Smectite clay Minerals: Properties and Uses. Philos. Trans. R. Soc. Lond. Math. Phys. Eng. Sci. 311, 391–409.

Offre, P., Spang, A., Schleper, C., 2013. Archaea in Biogeochemical Cycles. Annu. Rev. Microbiol. 67, 437–457.

Pedersen, R.B., Rapp, H.T., Thorseth, I.H., Lilley, M.D., Barriga, F.J.A.S., Baumberger, T., Flesland, K., Fonseca, R., Früh-Green, G.L., Jorgensen, S.L., 2010a. Discovery of a black smoker vent field and vent fauna at the Arctic Mid-Ocean Ridge. Nat. Commun. 1, 126.

Pedersen, R.B., Thorseth, I.H., NygåRd, T.E., Lilley, M.D., Kelley, D.S., 2010b. Hydrothermal Activity at the Arctic Mid-Ocean Ridges, in: Rona, P.A., Devey, C.W., Dyment, J., Murton, B.J. (Eds.), Diversity Of Hydrothermal Systems On Slow Spreading Ocean Ridges. American Geophysical Union, pp. 67–89.

Percival, J., B., Ames, D., E., 1993. Clay mineralogy of active hydrothermal chimneys and an associated mound, Middle Valley, Northern Juan de Fuca Ridge. The Canadian Mineralogist, pp. 957-971

Petersen, S., Krätschell, A., Augustin, N., Jamieson, J., Hein, J.R., Hannington, M.D., 2016. News from the seabed – Geological characteristics and resource potential of deep-sea mineral resources. Mar. Policy 70, 175–187.

Picard, A., Kappler, A., Schmid, G., Quaroni, L., Obst, M., 2015. Experimental diagenesis of organo-mineral structures formed by microaerophilic Fe(II)-oxidizing bacteria. Nat. Commun. 6, 6277.

Rhizosphere Research Products-for Rhizon samplers-home [WWW Document]. URL http://www.rhizosphere.com/ (accessed 10.30.16).

Rimstidt, J.D., Chermak, J.A., Gagen, P.M., 1993. Rates of Reaction of Galena, Sphalerite, Chalcopyrite, and Arsenopyrite with Fe(III) in Acidic Solutions, in: Alpers, C.N., Blowes, D.W. (Eds.), Environmental Geochemistry of Sulfide Oxidation. American Chemical Society, Washington, DC, pp. 2–13.

Roalkvam, I., Jørgensen, S.L., Chen, Y., Stokke, R., Dahle, H., Hocking, W.P., Lanzén, A., Haflidason, H., Steen, I.H., 2011. New insight into stratification of anaerobic methanotrophs in cold seep sediments: Sedimentary stratification of methanotrophs. FEMS Microbiol. Ecol. 78, 233–243.

Rona, P.A., 2003. Resources of the sea floor. Science 299, 673–674.

Sekiguchi, Y., Muramatsu, M., Imachi, H., Narihiro, T., Ohashi, A., Harada, H., Hanada, S., Kamagata, Y., 2008. Thermodesulfovibrio aggregans sp. nov. and Thermodesulfovibrio thiophilus sp. nov., anaerobic, thermophilic, sulfate-reducing bacteria isolated from thermophilic methanogenic sludge, and emended description of the genus Thermodesulfovibrio. Int. J. Syst. Evol. Microbiol. 58, 2541–2548.

Sidenko, N.V., Sherriff, B.L., 2005. The attenuation of Ni, Zn and Cu, by secondary Fe phases of different crystallinity from surface and ground water of two sulfide mine tailings in Manitoba, Canada. Appl. Geochem. 20, 1180–1194.

Singer, P.C., Stumm, W., 1970. Acidic Mine Drainage: The Rate-Determning Step. Science 176, 1121-1123

Slobodkina, G.B., Kolganova, T.V., Chernyh, N.A., Querellou, J., Bonch-Osmolovskaya, E.A., Slobodkin, A.I., 2009. Deferribacter autotrophicus sp. nov., an iron(III)-reducing bacterium from a deep-sea hydrothermal vent. Int. J. Syst. Evol. Microbiol. 59, 1508–1512.

Smuda, J., Dold, B., Friese, K., Morgenstern, P., Glaesser, W., 2007. Mineralogical and geochemical study of element mobility at the sulfide-rich Excelsior waste rock dump from the polymetallic Zn–Pb–(Ag–Bi–Cu) deposit, Cerro de Pasco, Peru. J. Geochem. Explor. 92, 97–110.

Steen, I.H., Dahle, H., Stokke, R., Roalkvam, I., Daae, F.-L., Rapp, H.T., Pedersen, R.B., Thorseth, I.H., 2016. Novel Barite Chimneys at the Loki's Castle Vent Field Shed Light on Key Factors Shaping Microbial Communities and Functions in Hydrothermal Systems. Front. Microbiol. 6.

Takai, K., 2006. Sulfurimonas paralvinellae sp. nov., a novel mesophilic, hydrogen- and sulfur-oxidizing chemolithoautotroph within the Epsilonproteobacteria isolated from a deep-sea hydrothermal vent polychaete nest, reclassification of Thiomicrospira denitrificans as Sulfurimonas denitrificans comb. nov. and emended description of the genus Sulfurimonas. Int. J. Syst. Evol. Microbiol. 56, 1725–1733.

Thorez, J., 1975. phyllosilicates and clay minerals, a handbook for their laboratory x-ray diffraction analysis, 1st ed. G. Lelotte.

Van Dover, C.L., 2011. Tighten regulations on deep-sea mining. Nature 470, 31–33.

Weber, K.A., Achenbach, L.A., Coates, J.D., 2006. Microorganisms pumping iron: anaerobic microbial iron oxidation and reduction. Nat. Rev. Microbiol. 4, 752–764.

Yamabi, S., Imai, H., 2002. Growth conditions for wurtzite zinc oxide films in aqueous solutions. J. Mater. Chem. 12, 3773–3778.

Appendix

A: Pictures of the sediment cores

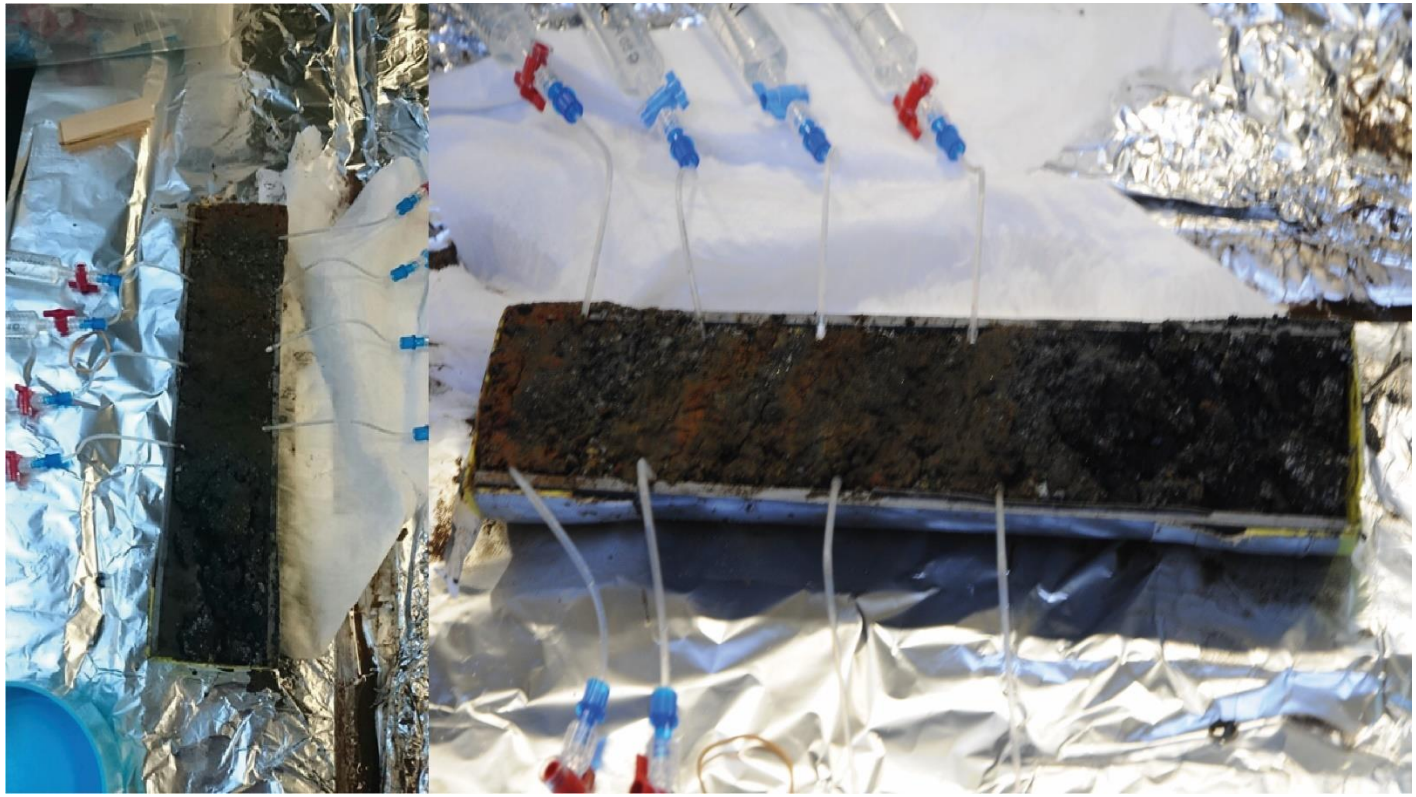

Figure A-1: Picture of core 1 (mound material) after it has been split in half, during pore-water extraction.

Figure A-2: The background sediment (core 2) during XRF core scan. Pore-water has not been extracted.

B: Microbial community structure

Table 5*:* Classification down to class level in both sediment cores. Red star indicates poly deoxyinosinic-deoxyidylic acid treatment. Remaining samples in core 1 are treated with poly adenosine. Samples from core 2 have not gone through treatment before DNA extraction. "Unassigned;Other;Other» contains unassigned sequences, whilst «Other: <5%» contains classified sequences which are compiled due to low relative abundance. Note: Green Genes database.

	Core 1, depth (cm)							Core 2, depth (cm)									
	0.1	0.1*	1	11	11	18	25	0.1	0.1	2	2	5	15	20	20	48	48
Class	Relative abundance (%)							Relative abundance (%)									
k__Archaea;p__Crenarchaeota;c__MBGB	0	0	0.7	0.2	0.1	0.2	0.2	0	0	0	0	0	0	0	0	0	0
k__Archaea;p__Crenarchaeota;c__MCG	0.1	0	0.3	0.5	0.3	0.3	0.5	0	0	0	0	0	0	0	0	0	0
k__Archaea;p__Crenarchaeota;c__Thaumarchaeota	12	11.2	1.5	0.5	0.3	1.7	2.3	26.1	21.5	21.5	23.5	23.2	17	15.4	13.7	16.1	17.2
k__Archaea;p__Crenarchaeota;c__THSCG	0	0	0	0	0	0	0.5	0	0	0	0	0	0	0	0	0	0
k__Archaea;p__Euryarchaeota;c__Thermoplasmata	0	0	0.5	0.5	0.5	0.6	1.2	0	0	0	0	0	0	0	0	0	0
k__Bacteria;p__;c__	0.7	0.7	1.2	3.2	2.5	1.8	1.2	0	0	0.1	0.1	0.1	0.1	0.1	0	0.3	0.2
k__Bacteria;p__Acidobacteria;c__	1.1	0.8	0.1	0.1	0.1	0.3	0.4	0.8	0.9	0.9	1	1.2	0.5	0.8	1.1	0.2	0.2
k__Bacteria;p__Acidobacteria;c__Acidobacteria-6	0.5	0.6	0.6	0.1	0.1	0.2	0.2	1.6	1.6	1.5	1.7	1	0.6	0.6	0.7	0.6	0.7
k__Bacteria;p__Acidobacteria;c__BPC102	0.4	0.3	0.1	0.1	0	0.1	0.1	1.6	1.7	2.1	1.7	0.6	0.3	0.6	0.5	0.4	0.4
k__Bacteria;p__Acidobacteria;c__RB25	1.6	1.4	0.3	0.2	0.1	0.4	0.4	1.3	1.2	0.9	0.8	0.4	0.1	0.2	0.2	0.1	0.1
k__Bacteria;p__Acidobacteria;c__Sva0725	1.4	1.2	0.4	0	0	0.6	0.5	1.2	1.2	1.8	1.7	0.1	0.2	0.2	0.2	0.1	0.1
k__Bacteria;p__Actinobacteria;c__Acidimicrobiia	3.4	3.3	3	2.3	2.4	3.1	2.3	7.3	7	5.4	5.9	7	3.8	6.2	5.5	4	4.1
k__Bacteria;p__Actinobacteria;c__Actinobacteria	0.2	0.1	2.9	0.6	2.2	1.3	0.6	0	0	0	0	0	0.1	0.2	0.1	0.1	0.2

Class	Core 1, depth (cm)							Core 2, depth (cm)									
	0.1	0.1*	1	11	11	18	25	0.1	0.1	2	2	5	15	20	20	48	48
	Relative abundance (%)							Relative abundance (%)									
k__Bacteria;p__Actinobacteria;c__OPB41	0.1	0.1	1	0.8	1.1	2	0.6	0	0	0	0	0	0	0	0	0	0
k__Bacteria;p__Aquificae;c__Aquificae	0.1	0	0.1	0.1	0.2	0.1	9.5	0	0	0	0	0	0	0	0	0	0
k__Bacteria;p__Bacteroidetes;c__[Rhodothermi]	0.3	0.4	0.2	0.4	0.5	0.2	0.2	0.3	0.3	0.3	0.4	0	0.1	0	0	1.6	1.8
k__Bacteria;p__Bacteroidetes;c__Bacteroidia	0.1	0.1	1.5	1.4	1	1.6	2	0	0	0.1	0	0	0	0	0	0	0
k__Bacteria;p__Bacteroidetes;c__Cytophagia	0.9	1.1	0.5	0.1	0.2	0.5	0.4	0.7	0.7	0.7	0.7	0.1	0.2	0.6	0.2	0.2	0.2
k__Bacteria;p__Bacteroidetes;c__Flavobacteriia	0.3	0.5	0.3	0.1	0.1	0.4	0.2	0.2	0.2	0.1	0.1	0.1	0.1	0.1	0	0.1	0.1
k__Bacteria;p__Chlorobi;c__Ignavibacteria	0.1	0.1	1.2	0.4	0.8	0.7	0.1	0.1	0.1	0.1	0.1	0	0	0	0	0	0
k__Bacteria;p__Chloroflexi;c__Anaerolineae	0.2	0.2	2.7	1.3	1.6	1.5	1.3	0.1	0.1	0.2	0.3	0.6	1.9	0.5	0.5	0.6	0.5
k__Bacteria;p__Chloroflexi;c__Dehalococcoidetes	0.2	0.2	1.4	3.5	2.3	2	2.2	0	0	0	0	0	0	0	0	0	0
k__Bacteria;p__Chloroflexi;c__Ellin6529	1.4	1.6	1.4	4	3.9	1.4	0.6	0.2	0.3	0.4	0.3	0.2	0.1	0.1	0.2	0.1	0.1
k__Bacteria;p__Chloroflexi;c__S085	4.6	5	1.3	3	2.7	2.1	1	2.9	2.8	5.2	5.2	20.8	27.2	21.8	27.9	21.5	23.3
k__Bacteria;p__Chloroflexi;c__SAR202	2.1	2.9	0.8	0.7	0.6	0.8	0.7	2.9	3.3	5.3	5.3	7.6	8.4	9.2	8.7	10.5	10.2
k__Bacteria;p__Chloroflexi;c__TK17	1	1.4	0.5	0	0	0.4	0.2	1.2	1.2	1.3	1	0.7	0.5	1	0.9	0.4	0.2
k_Bacteria;p__Deferribacteres;c__Deferribacteres	0.8	1.0	4.6	5.7	6.4	5.4	8.6	0.3	0.4	0.5	0.5	0.4	0.8	0.9	0.4	0.8	0.5
k__Bacteria;p__Firmicutes;c__Clostridia	0.1	0	0.6	0.2	0.4	1.7	4.1	0	0	0	0	0	0	0	0	0	0
k__Bacteria;p__Gemmatimonadetes;c__Gemm-1	1.7	1.8	0.3	0.2	0.1	0.4	0.3	1.6	1.9	2.8	2.4	2.8	1.8	2.4	2.7	3	2.6
k__Bacteria;p__Gemmatimonadetes;c__Gemm-2	1.5	1.2	1.8	1.2	1.6	1.3	1.2	1.9	1.9	1.8	1.6	0.5	0.2	0.7	0.6	0.5	0.4

Class	Core 1, depth (cm)							Core 2, depth (cm)									
	0.1	0.1*	1	11	11	18	25	0.1	0.1	2	2	5	15	20	20	48	48
	Relative abundance (%)							Relative abundance (%)									
k__Bacteria;p__Gemmatimonadetes;c__Gemm-4	0.3	0.3	0.1	0.1	0.7	0.2	0.1	0.5	0.6	0.4	0.4	0.9	0.4	1	1.4	0.2	0.3
k__Bacteria;p__Gemmatimonadetes;c__Gemm-6	0	0	0	0	0	0	0	0.2	0.1	0.2	0.2	0.3	0.3	0.6	0.7	0.2	0.1
k__Bacteria;p__GN02;c__GN07	0	0	0.5	0.2	0.2	0.4	0	0	0	0	0	0	0	0	0	0	0
k__Bacteria;p__GN04;c__GN15	0.3	0.8	0.3	0.1	0.1	0.1	0.1	0	0	0	0	0	0	0	0	0	0
k__Bacteria;p__NC10;c__wb1-A12	0	0	0	0	0	0	0	0	0	0	0	0.1	0.4	0.5	0.5	0.3	0.3
k__Bacteria;p__Nitrospirae;c__Nitrospira	2.5	1.8	5.2	7.3	5.9	3.8	1.2	0.8	1.1	0.9	0.8	0.8	0.8	1.5	1.3	1.2	1
k__Bacteria;p__OP3;c__	0.1	0.1	0.6	0.4	0.4	0.9	0.7	0	0	0	0	0	0	0	0	0	0
k__Bacteria;p__OP3;c__BD4-9	0	0.1	0.5	0.9	1.1	0.9	0.5	0	0	0	0	0	0	0	0	0	0
k__Bacteria;p__OP3;c__koll11	0.1	0.2	0.3	0.5	0.3	0.4	0.3	0.3	0.3	0.5	0.6	0.2	0	0.3	0.2	0.6	0.5
k__Bacteria;p__OP8;c__OP8_1	0.5	0.3	3.6	5.1	4.6	3.4	2.5	0	0	0	0	0	0	0	0	0	0
k__Bacteria;p__OP9;c__JS1	0.2	0.1	2	1	1.3	3.3	2.4	0	0	0	0	0	0	0	0	0	0
k__Bacteria;p__Planctomycetes;c__OM190	0.9	0.9	0.1	0.1	0	0.4	0.4	0.7	0.8	0.5	0.5	0.1	0.1	0.1	0	0.1	0.1
k__Bacteria;p__Planctomycetes;c__Phycisphaerae	1.8	2	4.1	6.9	5.1	4.5	5.9	2.8	3.2	3.1	3	0.8	1.3	1.4	1.2	1.5	1.6
k__Bacteria;p__Planctomycetes;c__Pla3	0.1	0.1	0	0	0	0.1	0.1	0.2	0.3	0.3	0.2	0.2	0.1	0.2	0.1	0.1	0.1
k__Bacteria;p__Planctomycetes;c__Planctomycetia	3.9	3.3	5.8	12.5	13.1	4.4	1.8	1.8	2.1	1.4	1.5	0.2	0.4	0.4	0.3	0.5	0.4
k__Bacteria;p__Proteobacteria;c__Alphaproteobacteria	6.5	8.2	4.2	6.9	7.3	6.2	2.9	6.6	6.8	8.4	8	9.7	14.6	11.2	10.8	15.2	15.7
k__Bacteria;p__Proteobacteria;c__Betaproteobacteria	0.6	0.7	0.7	0.2	0.5	0.5	0.7	0.8	1	0.4	0.5	0.2	0.5	0.4	0.3	0.5	0.5
k__Bacteria;p__Proteobacteria;c__Deltaproteobacteria	6.6	6.1	9.8	8.3	7.7	10.5	11	7.5	8.8	7.8	7	4.9	5.1	5.1	5.2	3.7	3.2
k__Bacteria;p__Proteobacteria;c__Epsilonproteobacteria	0	0.1	0.1	0.2	0.1	0.8	0.2	0	0	0	0.1	0	0	0	0	0	0
k__Bacteria;p__Proteobacteria;c__Gammaproteobacteria	32.9	32.1	15	5.8	8.3	14.3	14.6	20.9	20.8	17.5	17.9	10.6	6.9	9.2	10.1	7.4	6.4

Class	Core 1, depth (cm)							Core 2, depth (cm)									
	0.1	0.1*	1	11	11	18	25	0.1	0.1	2	2	5	15	20	20	48	48
	Relative abundance (%)							Relative abundance (%)									
k__Bacteria;p__SAR406;c__AB16	0.4	0.4	4.1	5	5.6	4.7	7.9	0	0	0.1	0.1	0.1	0.7	0.6	0.3	0.5	0.3
k__Bacteria;p__SBR1093;c__VHS-B5-50	0.2	0.2	0.3	0.3	0.2	0.1	0.1	0.7	1	1	0.7	0.7	0.6	0.8	0.6	0.2	0.3
k__Bacteria;p__Spirochaetes;c__Spirochaetes	0.1	0.1	0.3	0.5	0.3	0.3	0.2	0	0	0	0	0	0	0	0	0	0
k__Bacteria;p__TM6;c__SJA-4	0.2	0.1	1.9	0.9	0.8	0.5	0.2	0.2	0.2	0.2	0.3	0	0.1	0.2	0.1	0	0
k__Bacteria;p__WS3;c__PRR-12	0.4	0.2	0.4	0.4	0.4	0.5	0.5	0.3	0.4	0.3	0.2	0.1	0	0.2	0.1	0.1	0.1
Unassigned;Other;Other	1.9	2.1	6.9	4.9	4.7	4.4	4.6	0.7	0.9	1	1.1	0.8	1.8	2.5	1.3	4	3.3
Other: <0.5% compiled	2.8	2.8	4.7	4.9	5.1	5.6	5.1	2	2.7	2.7	2.6	1.5	2	2.5	1.5	2.6	2.8
Total:	99.4	99.3	98.7	99.1	99.5	98.9	99	99	99	99.2	99.5	99.2	99.3	99.4	99.7	99.3	99.6

C: DNA isolation and PCR amplification

December 2015 – January 2016

DNA extraction using FastDNA Spin Kit for Soil

0.25-0.5 g of sample material where put in a Lysis E Matrix tube following the manufacturers protocol with minor adjustments.

Protocol following Lot.nr 68505, with the minor adjustment:

- Vortex the sample between step 3 and 4.
- Step 4: "Homogenize in the FastPrep instrument for 30 seconds…"
- Step 5: "Centrifuge at 14,000 x g for 8 minutes…"
- Step 9: "…Place tube in a rack for 6 minutes to allow…."
- Step 10: "Remove and discard 600 µL…"
- Step 16: "Gently resuspend the Binding Matrix (above the SPIN filter) in 100 µL…"
- Step 17: "Centrifuge at 14,000 x g for 1 minute with open tube…"

The isolated DNA was eluted in 100 µl DNase free water and quantified by Quantus Flurometer (Promega BioSystem Sunnyvale, Sunnyvale Inc, USA) and stored at -20°C before PCR amplification. After storage at -20°C the isolated DNA templates were amplified by a two-step PCR approach using universal 16S rRNA primers together with HotStarTaq® PCR kit (Qiagen). The procedure was done following the manufacturers protocol.

PCR amplification of the extracted DNA

PCR Step 1

Each sample was amplified in triplicates.

- 2.5µl template, 12.500µl 2MMxHotStar Taq® Master Mix kit, 9.750µl DNase Free water and 0.125µl of each primer (519F: CAGCMGCCGCGGTAA, 806R: CACTACHVGGGTATCTAATCC) adding up to a total volume of 25µl.

- Thermal cycling program:
    - 95°C for 15minutes
    - 30 X (94°C for 30 seconds, 56°C for 30 seconds and 72°C for 1.5 minutes) and
    - 72°C for 7 minutes
    - Cool down to 4°C.
- The triplicates were pooled and purified using Agencourt®AMPure®XP (Beckman Coulter, lot.nr: 14371200).
- DNA quantification was performed with Quantus Flurometer (Promega BioSystem Sunnyvale, Sunnyvale Inc, USA) or by visual inspection using 1D gel electrophoreses (Agarose, Electran, Prod.nr: 43879).

PCR Step 2

- 10µl of each PCR1 template was used with 2.0µl 519F including a MID sEquence of 44pb, 0.20µl 806R w/adapter, 12.50µl 2MMxHotStar Taq® Master Mix and 0.30 µl DNase Free water, adding up to a volume of 25µl.
- Thermal cycling program:
    - 95°C for 15 minutes
    - 7 X (94°C for 30 seconds, 56°C for 30 seconds and 72°C for 1.5 minutes)
    - 72°C for 7 minutes
    - Cool down to 4°C.
- Results were purified and quantified following the same procedure as after step 1.